The Effects of Pore Fluid Pressure on the Frictional Behavior of Antigorite Serpentinite: Implications for Slow Slip on Subduction Zone Faults

Ben Belzer

April 25th, 2016

Advisors:

Dr. Melodie French

Dr. Wenlu Zhu

GEOL394

Abstract

Changes in slip rate can change the coefficient of friction on the fault surface. If the frictional strength on a fault increases with increased velocity, then the fault stabilizes with acceleration, and we identify this behavior as velocity-strengthening. If the frictional strength decreases with increased velocity, then the fault could be prone to unstable slip, and we identify this potential for instability as velocity-weakening. This endmember model of the velocity dependence of friction is a robust first order tool for quantifying the potential for stable aseismic creep or earthquakes along a fault. However, the recent discovery of slow slip events (i.e. episodic tremor and slip) in subduction zones has posed nuance to this standard model. Slow slip events display intermediate behavior between abrupt, unstable earthquakes and aseismic creep. These events are slow, prolonged, periodic, and though they are not themselves destructive, they are thought to increase stress updip on the subducting plate and potentially trigger violent earthquakes. To explain how frictional sliding processes regulate such transient behavior, it is thought that slow slip manifests from marginal velocity-weakening and/or transitions between velocity-weakening and velocity-strengthening. Although slow slip events occur over a wide range of temperature conditions and metamorphic facies, geophysical observations indicate that they are principally constrained within regions of low effective stress, induced by near-lithostatic pore fluid pressure [e.g. Kodaira et al. 2004; Peacock, 2009; Hawthorne and Rubin, 2010]. This study addresses the frictional and mechanical behavior of serpentine rich fault gouge experiencing relatively fast sliding velocities of slow slip at high fluid pressure and low effective stress. Using the hot-press triaxial deformation apparatus in the UMD Laboratory for Rock Physics, I conduct a series of friction tests on simulated fault gouge of antigorite serpentinite, a relevant lithology in subduction zones. Variations in frictional behavior and dilatancy are documented at various pore fluid pressures and effective stresses, which reveal the following. First is an observed dependence of frictional behavior on effective stress, in which low effective stress favors velocity-strengthening and high effective stress favors velocity-weakening. Second is enhanced velocity-strengthening with elevations in pore fluid pressure and confining pressure, independent of (i.e. with negligible change in) effective stress. These observations imply that heterogeneities of fluid pressure within slow slip regions could control variations in slip activity. However, the latter results also reveal difficulty in using the effective stress law to extrapolate frictional sliding processes at in situ pressures deep in the Earth's crust and mantle. Coupled with these implications, sudden increases in dilatancy and strain hardening rate are documented concurrently with pronounced velocity-weakening during one of the experiments, which brings to question dilatant hardening as an arresting mechanism of slow slip.

1. Table of Contents

2. Introduction

Several peer-reviewed papers that describe slow slip phenomena address how it has been one of the most exciting and revolutionary discoveries in solid earth geophysics in recent decades [e.g. Peng, et al. 2010]. First detected by continuous GPS networks, slow slip events are now known to occur in multiple subduction zones such as in Cascadia [Dragert et al. 2001], southwest Japan [Miyazaki et al., 2006], Mexico [Kostoglodov et al. 2003], New Zealand [Douglas et al. 2005], and Alaska [Ohta et al., 2006]. As illustrated schematically in *Figure 1*, slow slip events occur between 30-50 km depth and are thought to increase normal stress updip on the locked segment of the subducting plate. [Shelly and Johnson, 2011]. Studies of slow slip phenomena are therefore important for evaluating triggers of large earthquakes, including past megathrust events in Japan [Ito et al., 2013] or future events in Cascadia [Chapman and Melbourne, 2009].

The intermediate behavior of slow slip phenomena is observed as follows: average slip rates are 10^{-8} to 10^{-7} m/s, which are many orders of magnitude slower than the sudden rupture of an earthquake, yet faster than aseismic plate velocities by 1-2 orders of magnitude [Rogers and Dragert, 2003]. Occurrences of slow slip are also periodic and are often accompanied by non-volcanic tremor – leading to its designation as episodic tremor and slip (ETS) [Obara et al., 2004]. (3) The duration of slip varies from days to years, and the recurrence interval is on the order of months to years [Schwartz and Rokosky, 2007].

The estimated temperatures at which slow slip occurs vary between 300-500^{o}C, corresponding with a wide range of metamorphic facies [Peacock, 2009]. High Vp/Vs ratios observed at the approximate locations of ETS indicate that slow slip occurs in regions of high

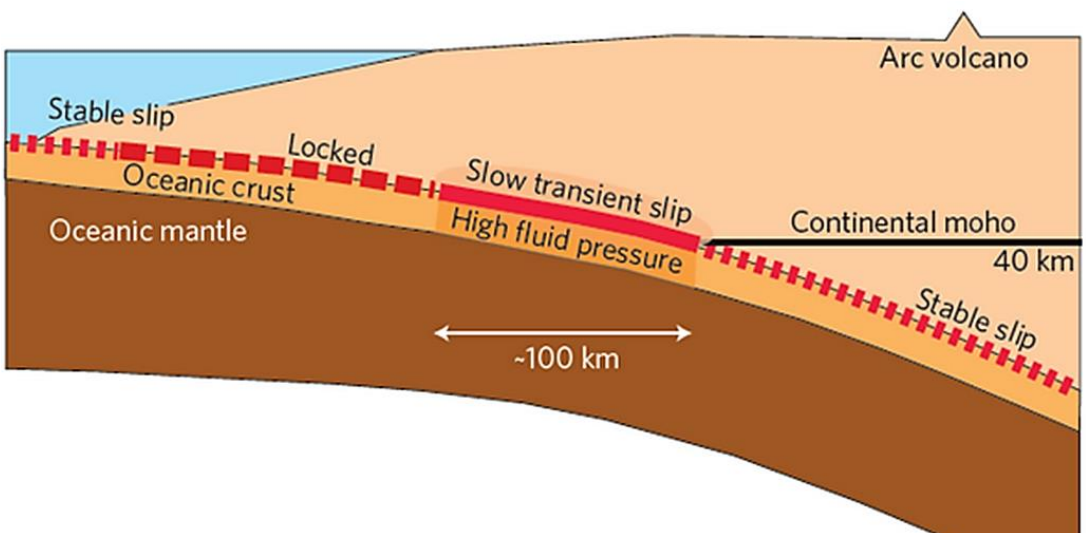

Figure 1: Profile of the Cascadia subduction zone showing slip behavioral transitions along the plate interface with depth. Labelled above are the upper seismogenic zone, middle zone of transient slip, and downdip aseismic slip zone. The locked, seismogenic zone is associated with unstable, stick-slip and is a host for megathrust earthquakes. Beneath this zone, transient slow slip is thought to increase stress updip on the locked section (Adapted from Peng, et al., 2010).

pore fluid pressure, where fluid is supplied by the dehydration of water-bearing minerals during prograde metamorphic reactions [e.g. Kodaira et al. 2004; Peacock, 2009]. Furthermore, seismological studies show that the tremor associated with slow slip modulates sensitively to tidal action, suggesting evidence of near-lithostatic pore fluid pressure with very low effective normal stress (<5 MPa) [Hawthorne and Rubin, 2010]. Considering that for the Earth's crust, the relation between lithostatic pressure and depth is roughly 1 GPa or 10 kbar per 35-40 km, near-lithostatic pore fluid pressure is remarkable.

3. Background

Although it is well understood that elevated pore pressure reduces frictional strength along faults (by decreasing effective normal stress), there are few documented studies on the rate and state friction of a serpentinite fault at variable fluid pressure. How the coefficient of friction on the fault interface behaves in terms of velocity-strengthening or velocity-weakening addresses the fault's potential for stable or unstable slip. If high pore fluid pressure is indeed a condition at the approximate locations of slow slip, then it is important to investigate the influence of variable pore pressure on the friction velocity dependence of serpentinite. To provide context for the scope of this study, the following sections describe rate and state friction, the effects of pore fluid pressure, and the choice of antigorite serpentinite.

3.1. Rate and state friction

To model real earthquakes and faulting processes from friction experiments in the laboratory, workers have conventionally used rate and state variable friction relations [e.g. Ben-Zion and Rice, 1997]. Rate and state friction describes the observed transient and steady-state effects of changes in sliding velocity on the friction coefficient. These relations were first developed from laboratory observations to explain how sliding behaviors varied on a simulated fault [Dieterich 1979]. There are several formulations of rate and state friction. These friction relations describe a dependence of friction coefficient on slip rate and dependence on displacement or time [Ruina 1983]. One of the first and still most commonly agreed upon friction relations is the Dieterich-Ruina law, which has the form [Scholz 1998]:

$$\tau = \left[\mu_o + a\, ln\left(\frac{V_f}{V_o}\right) + b\, ln\left(\frac{V_o\theta}{d_c}\right)\right]\sigma_n' \qquad (1)$$

In equation (1), a and b are material properties, V_f and V_o are the slip velocity and a reference velocity respectively, μ_o is the steady state friction when $V_f = V_o$, d_c is the critical slip distance, and θ is a state variable. In response to a sudden change in sliding velocity, the state variable evolves according to an aging law:

$$\frac{d\theta}{dt} = 1 - \frac{\theta V}{d_c} \qquad (2)$$

Equations (1) and (2) stipulate which variables are desired from laboratory testing. *Figure 2* illustrates how experimental results from a friction test yield the constitutive values *a* and *b* [Scholz 1998]. As shown schematically, the test imposes a sudden increase in loading velocity to measure the observed frictional response. The direct velocity response, which is the magnitude at which the friction changes from its initial steady state to peak stress, is designated by *a*. The evolutionary effect or the change in friction from peak stress to residual stress is designated by *b*. If *a* is observed to be greater than *b* (*a* - *b* > 0), this means the coefficient of friction increases with increasing velocity, and we document this response as velocity-strengthening. Conversely, if *a* is observed to be less than *b* (*a* - *b* < 0), the coefficient of friction decreases at that velocity step, and we document this response as velocity-weakening. Another important variable is the critical slip distance, d_c, which is typically observed in the range of μm to mm. This value is often interpreted as the minimum sliding distance required to renew the grain contact population [Scholz 1998]. In both diagrams, the initial and final load point velocities are 0.1 and 1.0 μm/s respectively. Note how these diagrams would appear if the velocity were to decrease by an order of magnitude (e.g. from 1.0 to 0.1 μm/s) instead. The rate and state figure would be inverted, but the difference between *a* and *b* would remain the same.

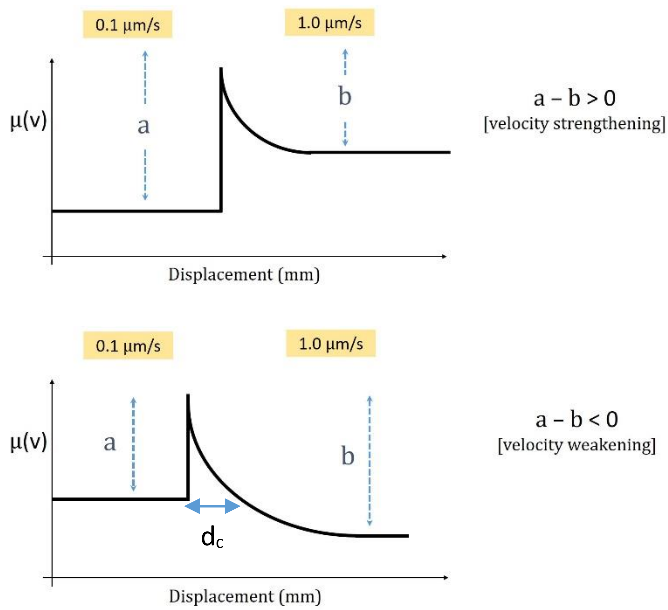

Figure 2. A schematic diagram showing velocity-strengthening and velocity-weakening behavior. The friction coefficient strengthens with increasing velocity if a > b and weakens with increasing velocity if a < b. Velocity-strengthening results in stable aseismic slip and velocity-weakening may cause unstable slip. The y-axis is the coefficient of friction and the x-axis is the displacement in millimeters along the fault plane.

The difference between *a* and *b* is a robust first order tool for quantifying the potential for stable aseismic creep or stick-slip motion along a fault. This is because only stable sliding is possible when the friction is velocity-strengthening. However, when the friction is velocity-weakening, sliding can be either stable or unstable. Unstable slip occurs if the decrease of friction is more rapid than elastic unloading [Marone et al, 1990]. Stable slip within the velocity-weakening regime occurs if the frictional decrease is less rapid than elastic unloading of the system. From equation (1), we can calculate the velocity dependence of friction, *a-b*, using the following calculation

$$\frac{d\mu_{ss}}{d(lnV)} = a - b \qquad (3)$$

The calculated value of *a-b* describes the material's frictional sliding behavior. Depending on the study, the analysis and interpretation of frictional behavior may involve plotting *a-b* as a function of displacement, sliding velocity, and/or other variables of interest (e.g. normal stress [Mair and Marone, 1999], temperature [Lockner et al., 1986], composition of gouge mixture [Moore and Lockner, 2011], etc.).

3.2. Importance of pore fluid pressure

Pore fluid pressure is the pressure of the fluid within the rock's pores (i.e. the stress applied to the inner walls of the pore space). Because pressure is a scalar quantity defined as force per unit area, pore fluid pressure is inversely proportional to pore volume in undrained conditions. That is, the fluid pressure increases when compaction reduces pore volume faster than fluid can flow out of the rock. Conversely, the fluid pressure decreases when dilation expands pore volume faster than fluid can flow in. Pore fluid pressure is an important variable in rock mechanics because it counteracts the stress applied to the rock, as illustrated schematically in *Figure 3*. At any point in a rock body, the vertical stress is equal to the weight of overlying material, and a principal stress tensor defines the 3-dimensional stress state of the rock. The difference between the normal stress, which is the load force applied perpendicularly to the surface area, and the pore fluid pressure is the effective normal stress σ_e. As the modifier implies, this is the actual stress experienced by the rock itself. The mathematical relationship between pore fluid pressure and normal stress is:

$$\sigma_e = (\sigma_n - P_f) \qquad (4)$$

where P_f is pore fluid pressure, σ_n is normal stress, and σ_e is the effective normal stress. Each of these variables can be expressed in units of MPa or psi. Ultimately, effective normal stress is a critical variable in earthquake studies because of its influence on fault strength. When pressure conditions allow for greater effective stress, fault reactivation in turn requires greater shear stress (i.e. force applied parallel to the fault surface) to overcome friction. Conversely, elevated pore fluid pressure is well-known to weaken frictional shear resistance along a fault by decreasing effective normal stress. This phenomenon is represented mathematically by:

$$\tau\,(v) = \mu\,(v) * \sigma_n' \quad \text{or}$$

$$\tau\,(v) = \mu\,(v) * (\sigma_n - P_f) \qquad (5)$$

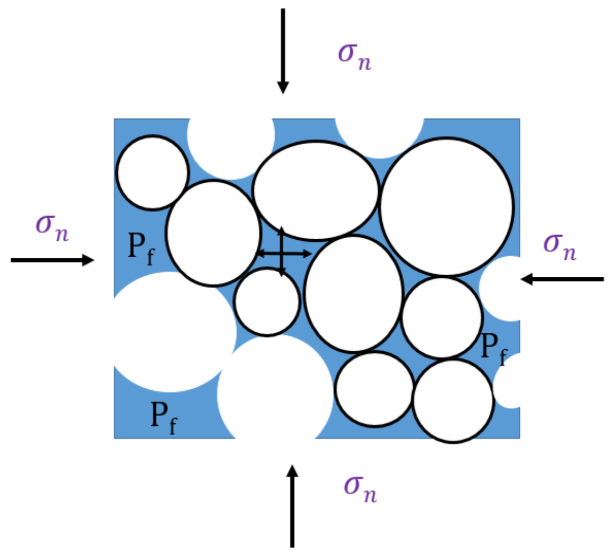

Figure 3: A cartoon schematically showing the counteraction between normal stress and pore fluid pressure. Pore fluid (blue) occupies void spaces between grains (white) in a rock. The pore fluid pressure is denoted as P_f, which applies stress against the inner walls of the pore space. Its stress vectors are depicted as crossed double arrows. Labelled outside the field of view are normal stresses, which apply stress in the opposite direction.

where τ is the frictional shear resistance and μ is the coefficient of friction. Note the similarity and difference between equations (1) and (5). The friction coefficient, defined as the ratio of shear stress to normal stress, is a physical property of the rock and depends on velocity and temperature.

$$\mu = \sigma_s / \sigma_n \qquad (6)$$

The velocity dependence of friction is modelled by rate and state variable friction laws, which relate a material's frictional behavior to its velocity and slip history. Although workers have documented the effects of temperature and normal stress on the frictional sliding behavior of various lithologies [e.g. Chester, 1994; Scholz, 1998], the effects of pore fluid pressure on the frictional behavior of serpentinite remain unresolved.

The primary objective of this study is to address whether relationships exist between pore fluid pressure and frictional sliding processes. To infer if additional mechanisms trigger or arrest slow slip, however, it is also helpful to document and assess mechanical changes (e.g. dilatancy or compaction) within the deformed material. Although the following hypothesis lacks experimental evidence in phyllosilicate rocks, one of the proposed mechanisms for arresting slow slip before it accelerates to velocities typical of earthquakes is dilatant hardening [Segall et al., 2010]. As slow slip events nucleate and begin to accelerate from unstable friction, an increase in shear stress from sliding causes the pore volume of the rock (or gouge) to increase, which reduces the pore pressure in an undrained system. The reduction in fluid pressure caused by dilation causes an increase in the effective normal stress, causing the shear strength of the rock to increase (i.e. harden).

3.3. Justification of antigorite serpentinite

Verde Antique Serpentinite is chosen for this experimental study for several reasons. Serpentinite is an abundant phyllosilicate-rich rock in subduction zones, and slow slip is inferred to occur in phyllosilicate-bearing rocks [Shelly et al., 2009]. Because serpentinite is formed by the hydration and alteration of mantle rocks at temperatures below 500-600°C (Evans et al., 1976), it is contained within most of the altered portion of subducting oceanic crust and mantle. Moreover, the Verde Antique Serpentinite is composed dominantly of antigorite, which is the highest pressure and temperature member of the serpentine group – $Mg_3Si_2O_5(OH)_4$ – and therefore the main component of prograde serpentinites in subduction zones [Wicks and Whittaker, 1977]. Antigorite is stable up to pressures and temperatures of 6 GPa and 650°C [Ulmer and Trommsdorff, 1995] – beyond which, it dehydrates to form olivine and other products. Antigorite's high P-T stability range permits it to be both a major water carrier and a commonly occurring phyllosilicate in the subducting plate. The latter characteristic is important because ETS observations occur all throughout the greenschist, blueschist, and amphibolite metamorphic facies, indicating that slow slip processes are not directly controlled by a specific temperature or metamorphic reaction [Peacock, 2009]. From an experimental approach, testing the frictional properties of antigorite serpentinite could provide more applicable results than testing that of an overlying and more petrologically constrained metasedimentary rock, like blueschist or amphibolite.

Additional motivations to test the Verde Antique are that the serpentinite is readily available and that other workers have tested its mechanical and frictional properties (or at least that of similar antigorite serpentinite at various strain-rates and P-T conditions [e.g. Reinen et al. 1991, Okazaki et al. 2015]. The merit of testing Verde Antique is that there is already groundwork laid out, providing a more complete frame of reference.

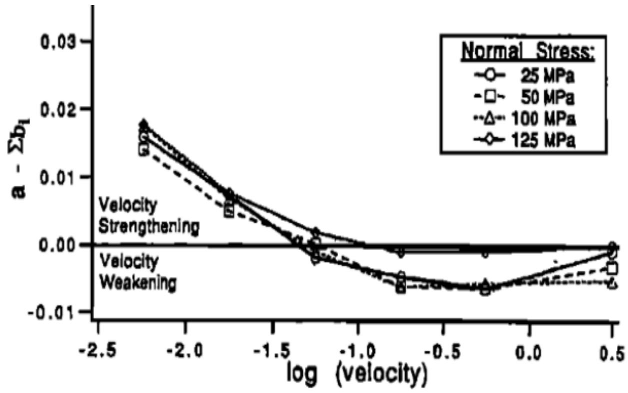

Figure 4: A previous study on antigorite serpentinite, comparing a-b behavior as a function of velocity at four effective stresses (25 MPa, 50 MPa, 100 MPa, 125 MPa).

3.4. Previous studies on serpentinite

Previous experimental work on antigorite serpentinite is depicted in *Figures 4* and *5*, selected from Reinen [1994] and Okazaki [2015], respectively. In both studies, friction tests were conducted on fault gouge of antigorite serpentinite. Fault gouge is a crushed, very fine-grained rock naturally formed by friction along a fault boundary as the fault moves. Gouge is prepared for laboratory testing by grinding a rock sample to very small grain sizes, usually smaller than <150 µm. *Figure 4* shows *a-b* as a function of loading velocity during four experiments at variable normal stress. The plotted results show a general transition in the Verde Antique gouge from velocity-strengthening behavior at slow loading velocities to velocity-weakening behavior at fast loading velocities. The transition occurs within the range of 0.032 to 0.10 µm/s. Note these loading velocities are relevant to slow slip events, which are endmembered kinematically between stable aseismic slip and unstable stick-slip events that produce earthquakes. Because slow slip behaves intermediately between these endmembers, slow slip events could be manifestations of transitions in

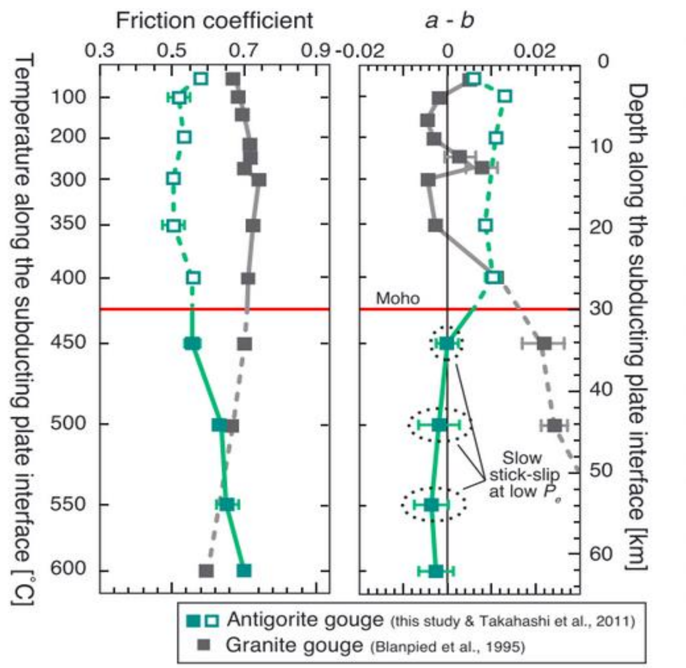

Figure 5: Previous experimental work on antigorite serpentinite, comparing the frictional properties of antigorite serpentinite (green) with those of granite gouge (gray) obtained by Blanpied et.al [1995]. The left-hand diagram plots the friction coefficient as a function of temperature (left y-axis) which is also correlated to depth (right y-axis). The Moho is represented by the red line at 30 km. The right-hand diagram plots the changing behavior of *a-b* along the same y-axes.

frictional behavior. In addition, *Figure 5* indicates that slow slip could manifest from marginal velocity-weakening. Okazaki et al [2015] displays two separate plots of the friction coefficient and *a-b* as a function of temperature and correlated depth along the subducting plate interface. The serpentinite friction data (in green) were obtained by testing antigorite serpentinite sampled from Japan's Nomo metamorphic belt. The plot shows a transition in the serpentinite gouge from velocity-strengthening behavior at shallow depths to marginal velocity-weakening behavior at depths relevant to slow slip processes. The values between depths of 30-55 km are circled to suggest slow stick-slip at low effective pressure. Error bars show ambiguity, however, in the frictional behavior.

Recall that high Vp/Vs ratios at the approximate depths of ETS indicate that slow slip occurs in regions of near-lithostatic pore fluid pressure (e.g. Kodaira et al. 2004). The right-hand plot in *Figure 5* is unique because it designates *a-b* values representative of slow slip, and it correlates subduction zone depths with velocity-strengthening and velocity-weakening in serpentinite. However, the effects of pore fluid pressure on frictional sliding processes at depths relevant to slow slip have yet to be addressed.

4. Hypotheses

In this thesis research, I document the frictional and mechanical behavior of antigorite serpentinite gouge experiencing fast sliding velocities of slow slip at variable fluid pressure and effective normal stress. My hypotheses are:

1) Increasing pore fluid pressure enhances the velocity-strengthening regime of a serpentinite fault, promoting the potential for stable slip.

2) Increasing pore fluid pressure does not influence the frictional velocity dependence of a serpentinite fault (null hypothesis).

3) Serpentinite gouge dilates in the velocity-weakening regime, supporting dilatant hardening as a mechanism which stabilizes acceleration along the fault

5. Experimental Methods and Design:

Using the hot-press triaxial deformation apparatus, I systematically compare the effects of variable pore fluid pressure on frictional behavior by imposing repeated step changes in loading velocity between each designed experiment. Pore fluid pressure is changed between each experiment to test the frictional behavior of serpentinite at 5 MPa, 65 MPa, 55 MPa, and 125 MPa with respective confining pressures of 75 MPa, 135 MPa, 65 MPa, and 135 MPa. Data from these friction tests are then analyzed to obtain *a-b* values in order to quantify velocity-strengthening and velocity-weakening behavior. I describe the mechanics of deformation by documenting the change in pore volume (i.e. how much the simulated gouge layer dilates or compacts), in conjunction with these frictional processes.

5.1. Preparing the serpentinite and driving blocks

The Verde Antique Serpentinite contains approximately 90% serpentine, 5% magnetite, and 5% magnesite [Reinen, 1991]. The magnesite occurs as white variably oriented veins, and the serpentine polymorph is antigorite, as determined through x-ray powder diffraction by Whittaker and Zussman [1956] and verified for the sample used in this study by French [2015]. As a carbonate phase, magnesite can dissolve more readily in a sample that is deformed at high enough temperature, possibly changing the overall mechanical behavior of the sample. To limit the mechanical effects of having a carbonate present, samples with the least amount of magnesite veins visible are selected and deformed at room-temperature.

To test its frictional behavior, I use two grams of serpentinite per experiment. Conceptually, the friction-test simulates a reactivated fault. Simulated gouge forms a layer along a 35° dipping fault between two driving blocks. During the experiment, deformation is fully accommodated by the gouge. In my experiments, I am using saw-cut Berea sandstone as the two driving blocks. This quartz arenite is mechanically stronger than the serpentinite and does not deform during the experiment. Moreover, its relatively high porosity (~ 20 %) and permeability enables sufficient draining to the gouge layer from the overlying pore fluid line [Zhu and Wong 1997]. The driving blocks of Berea sandstone are preordered and cut from a core sample that is approximately 50 mm in length and 25 mm in diameter. To create asperities on the fault boundary (so that shear occurs within the gouge layer and not at the boundary between the sandstone and gouge), I roughen the cut surfaces with 80 grit silicon carbide paper. I label the top and bottom blocks and measure their geometry with a 0.01 mm precision Vernier caliper. Further, I use a Mettler Toledo AG285 balance to measure the room-dry mass of each block before saturation.

To saturate the sandstone overnight, I place the two driving blocks in a beaker of distilled water within a vacuum chamber. Reducing the air pressure within the chamber forces air to move outside the pore space in the sandstone, enhancing saturation. The following day, I measure the mass of the saturated samples. Once these are measured and recorded, I can begin making the perfect serpentinite sandwich.

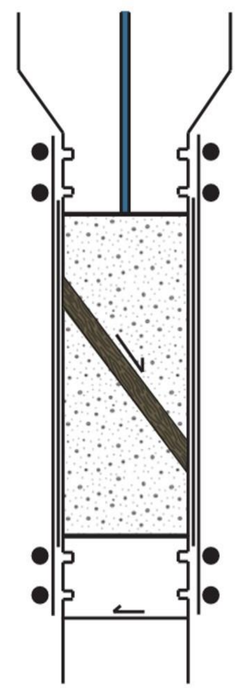

Figure 6: Cartoon schematic of the saw-cut sample used during the friction test. A poroelastic host rock (shown dotted above) is saw-cut to simulate a 30° dipping fault. As the sample is subjected to differential stress, slip is accommodated by the gouge layer (gray) between the driving blocks.

5.2. Sample assembly for friction test

To prepare the sample, I coat one millimeter of serpentinite gouge onto the fault surface of the lower driving block of sandstone (*Figure 7a*). After the gouge layer is spread, smoothed, and flush with the fault surface, I carefully slide the lower block into a green polyolefin jacket, cut approximately 7 cm in length. Subsequently, I insert the upper driving block to sandwich the serpentinite. An effective method to limit drag on the gouge before doing this last step is to cut open the jacket diagonally, so that it is parallel to the fault with one or two centimeters of overhang.

With the core sample aligned and jacketed, I add two $1^1/_4$ inch steel spacers – one overlying and one underlying the sandstone. Then, I place a $2^1/_4$ inch metal endcap in contact with the bottom spacer. The spacers contain a borehole (< 1 mm aperture) down its central axis. The side of the spacer that makes contact with the sandstone is indented with a combined pattern of crosshairs and concentric circles, as a means to equally distribute pore fluid from the borehole. To complete the assembly, I set the upper spacer in contact with the top endcap, which is already connected to a plug. Driving into the plug's center is high pressure tubing that transfers water down the borehole when attached to the pore fluid pressure line.

During the experiment, pore water must be the only fluid that enters the core sample. This means kerosene, which imposes confining pressure on the assembly when pressurized, must not leak in through the sides. Thus, I jacket the assembly, endcap-to-endcap, with clear polyolefin tubing approximately 13 cm in length (*7b*). I use a heat shrink gun to shrink the tubing tightly around the assembly. Then, I add a third and outermost jacket by repeating this process with slightly longer (~15 cm) black tubing. Finally, I fasten four steel tie wires, two above and two below each O-ring on the top and bottom endcaps, respectively (*7c*).

At this point, the assembly is ready to be loaded into the apparatus. To confirm that the latter is ready for the former, I check that the appropriate force gauge is connected and properly aligned with the axial piston to measure the load. I retract the axial piston, which is accomplished by turning the piston error signal down on the control panel, checking to make sure the servo is in displacement mode, and unlocking the piston. I manually pump the pore fluid pressure and check that water comes out from the open water line. After these items are accounted for, I screw the assembly into the top of the apparatus, with the lowermost endcap pointed down. Finally, I screw the high pressure tubing into a connector that is attached to the water line (*7d*).

5.3. Operating the triaxial deformation apparatus

The hot-press (*7e*) subjects cylindrical specimens to a triaxial stress state. A confining pressure is applied in the radial direction and is the minimum stress, and a piston is advanced in the axial direction to apply the maximum stress. The confining pressure is accommodated by kerosene which is filled and pressurized in the vessel chamber. During the experiment, the confining pressure is held constant in the vessel chamber while the axial piston is advanced to apply a measured, axial load. The difference between the axial load and the confining pressure is the differential stress, which is commonly designated as σ_1 - σ_3, and is what enables deformation of the sample to occur. Both the axisymmetric confining pressure and the axial load are controlled by corresponding piston cylinders, which are connected to a hydraulic pressure system. Also linked to the hydraulic system is an external pore fluid pressure system; pore water is collected outside the pressure vessel in a reservoir that controls the pore pressure and monitors the extruded volume of the fluid (i.e. the volume change of the specimen itself). As the specimen is deformed, the servo holds the pore pressure constant by advancing or retracting the piston to adjust the fluid supply. The imposed pressures, stress paths, and piston displacements are recorded during the experiment by linear voltage differential transformers (LVDTs) and pressure transducers. Each sensor designates a voltage channel that reads data into the computer. The data are recorded live into LabVIEW version 8.6.

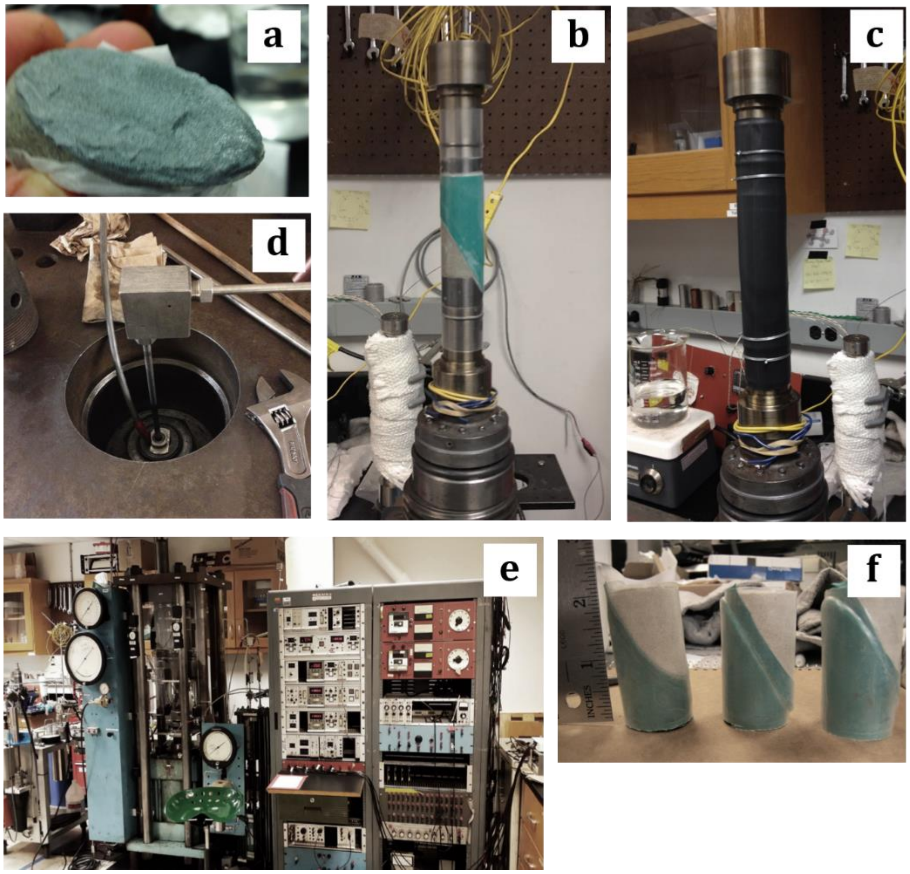

Figure 7: Photos of the sample preparation and apparatus setup: (a) shows 1mm of wet serpentinite fault gouge coated onto the surface of the lower sandstone driving block and not entirely smoothed yet, (b) shows the sample assembly with the two driving blocks, spacers, endcaps, green and clear polyolefin jackets, (c) shows the assembly with the black outermost jacket and tie wires added, (d) shows the assembly inverted, screwed in the top of the hot-press, and connected to the water line via high pressure tubing, (e) shows a wide view of the hot-press (left) and electronic panel with servo control system (right), and (f) shows the deformation of the sample after the friction test.

The day before the experiment, I load the sample into the apparatus, drain kerosene from the vent to fill the vessel chamber, and manually increase the confining pressure in 5 MPa increments up to approximately 20 MPa. Filling the vessel and applying pressure to the confining fluid is accomplished by opening hand valves connected to the kerosene supply, vent, and confining pressure piston. I also pump the pore fluid pressure a few times to saturate the sample. The wait time between increments to allow confining pressure to stabilize is four to five minutes. Subjecting the sample overnight to 20 MPa hydrostatic pressure allows the serpentinite grains to compact sufficiently and further removes asperities in the gouge layer. As observed the following day, the confining pressure equilibrates overnight typically to 15 MPa. The morning of the experiment, I save the data recorded from the night before and start a new recording in LabVIEW.

To set the experimental conditions for the friction test, I use the servo control system to increase the confining and pore fluid pressures to their desired magnitudes, which I then let stabilize for an hour. Then, I advance the piston at a constant axial displacement rate of 0.53 μm/s. I observe the load-cell reading in LabView to make note of the seal friction (i.e. the stress imposed by an o-ring seal), which is later subtracted from the stress on the force gauge to determine the axial stress on the sample. After recording the seal friction, I continue to advance the piston by the aforementioned rate. The stress on the force gauge increases linearly with displacement as the sample compacts, until eventually, the stress begins to curve and subside as the gouge friction decreases and stabilizes. When the friction is at steady state, I begin imposing sudden changes in loading velocity to record frictional velocity dependence. Between each step, I allow approximately 0.5 mm axial displacement, equally, to prevent displacement-dependent variation in slip history. The velocity steps I use in each experiment are: 0.53 μm/s → 0.12 μm/s → 1.24 μm/s → 4.94 μm/s → 1.24 μm/s → 0.12 μm/s → 1.24 μm/s. Experiments on samples VTG8 and VTG10 also repeat the fourth and fifth steps. After the last velocity step, I slowly reverse the piston (again at 0.53 μm/s) to reduce the axial stress and preserve microstructures that were created in the gouge layer. When the piston is no longer in contact with the sample, I increase the axial displacement rate. I use the servo control system to reduce the confining pressure and pore fluid pressure. Afterward, I empty the kerosene from the vessel chamber. I save and store the data in LabVIEW. Finally, I remove, clean, and disassemble the sample to store the deformed friction blocks, still contained by the inner two jackets (*7f*).

6. Methods of Analysis

6.1. Determining the friction coefficient

The experimental data consist of measurements of confining pressure, axial load, pore fluid pressure, and axial displacement. Obtaining the friction coefficient from the raw data involves a series of equations. These equations are calibrations of the instrument components and convert voltage measurements from the load cell and confining pressure channels to units of stress (MPa) and those from a LVDT on the main ram to axial displacement (mm).

The axial and radial stresses on the cylindrical sample are used to calculate the shear and normal stresses in the reference frame of the saw-cut (Appendix B, Equations *vi*-*xxi*). The differential stress on the one inch diameter cylindrical sample is determined from the output of the force gauge (*vi*), and it is equal to the applied axial stress minus the confining pressure and the stress imposed by an o-ring seal (*xiv*). The differential stress on the saw-cut sample is equal to the above divided by an additional area correction (*xviii*), which takes into account the decrease in the overlapping area of the saw-cut surfaces with increasing slip (*xvi*, *xvii*). The shear and normal stresses parallel to the saw-cut and within the gouge layer are calculated from the corrected differential stress path and known orientation of the saw-cut (*xix*, *xx*). The coefficient of friction is calculated by taking the ratio between the shear stress and the normal stress (*xxi*).

The evolution of friction coefficient with increasing shear displacement for each friction test is shown in section 8.1. The friction coefficient is plotted against shear displacement with a 0.5 second sampling rate, which provides approximately 30,000 relevant friction measurements on average per experiment. The data, including electronic noise contained in the original signal, are shown in grey.

6.2. Smoothing the friction data with a moving average

Although peaks and dips occur in short-term fluctuations uniformly through the signal, the high-frequency, high-amplitude noise is not conducive to visualizing (and documenting) the frictional behavior of the sample in response to the imposed velocity steps. I remedy this by using a for loop that runs a moving average on the entire time-series of friction. Given an original sequence a_n the n-moving average strings together a new sequence by taking the average of subsequences of n terms. For example, the smoothed sequence S_n using a rolling average of n = 2 or n = 3 is:

$$S_2 = \frac{1}{2}(a_1 + a_2,\ a_2 + a_3, \dots, a_{n-1} + a_n) \qquad or$$
$$S_3 = \frac{1}{3}(a_1 + a_2 + a_3,\ a_2 + a_3 + a_4, \dots, a_{n-2} + a_{n-1} + a_n) \quad (7)$$

I tested a number of subsequence lengths in the loop control statements, including n = 25, 50, 75, 100, 150, and 200 to see how averaging with different ranges affected the smoothing. As one would expect, moving larger average ranges through the signal removed more noise; however, applying an overly large smoothing range tended to distort (or ignore) the immediate frictional response and evolutionary effect at faster velocity steps. Through qualitative observation, I determined that n = 75 is a "goldilocks" subsequence size; the smoothed output of friction (shown in black in *Figure 9*) is neither too noisy nor too distorted.

6.3. Data correction for strain hardening

The serpentinite gouge strengthens with increasing strain (i.e. strain hardens) during all of the experiments, as represented by the nonlinear evolution of the friction coefficient with increasing shear displacement. By applying a slope correction that adjusts the data for linear increases in friction with displacement for each velocity step, I remove the superimposed effects of strain hardening. Piecewise slope corrections are used to model variations in horizontal, steady-state friction – thus isolating the velocity dependence of friction.

I correct for strain hardening as follows. For constrained regions in which the sample strain hardens at a constant rate, I first determine the slope of friction coefficient with displacement. Scatter plots are used to plot the coefficient of friction with shear displacement for these regions and show a linear equation – which contains the slope – and an R-squared for the line of best fit. R-squared values for the fitted lines used to correct strain hardening in sample VTG7 are shown in *Figure 8*. Given the slope of the best fit (m) and a series of shear displacement values (d) for the original friction series (μ_o), the corrected friction can be determined using the equation:

$$\mu_c = \mu_o - m * d \qquad (8)$$

One slope correction, however, does not fix all. The rate of strain hardening varies with the displacement rate and the amount of strain experienced by the sample. This requires that the correction process, as detailed above, be repeated for several segments of each friction path. Moreover, the original data series needs to be subdivided such that applying a new slope correction only affects the new subseries of data. Piecing together several subseries to model the entire friction path involves adjustments not only to *m* and *d*, which apply a new slope correction, but to μ_o as well, such as to negate the vertical displacement resulting from the slope correction. This endeavor is piecewise and somewhat tedious. *Figure 8* shows how segments of constant frictional growth from experiment VTG7 orient themselves after their individualized corrections are applied. The corrections are applied to both the linear growth in friction and the evolutionary effect preceding it, constructing a more accurate, composite model of rate and state frictional behavior.

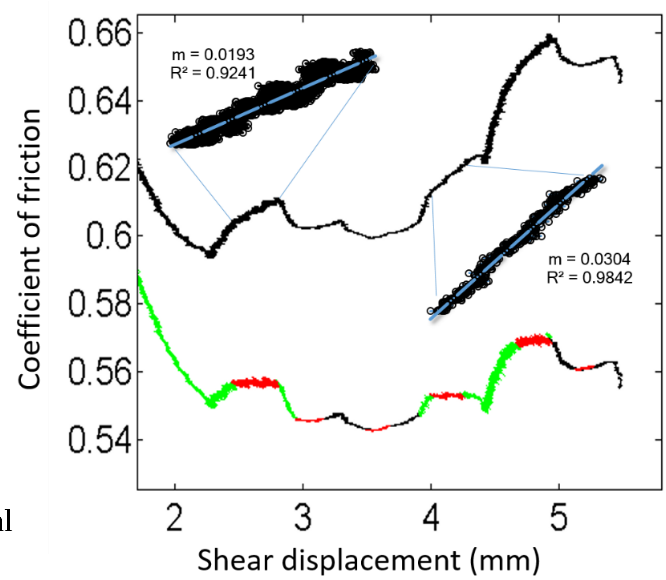

Figure 8. Example of strain hardening correction for VTG7. The slopes of linear increases in friction with displacement are measured to apply a slope correction to the data. The upper stress path is the observed friction coefficient. The original friction path is displayed in black and the corrected friction segments are displayed in green. Segments of steady-state friction averaged for *a-b* calculations are displayed in red. R-squared values for the displayed lines of best fit are 0.92 and 0.98.

6.4. Determining the velocity dependence of friction

After sequences within the data series are corrected to identify changes in steady-state friction, the modelled friction values are no longer representative of the actual value of the friction coefficient. However, when ascertaining the velocity dependence of friction, this is conveniently a non-issue. Actual values of friction are not required in analyzing the frictional behavior of the sample. Only the difference in steady-state friction and the natural logarithm of the velocity quotient are essential, as shown by the following equation:

$$a - b = \frac{d\mu_{ss}}{ln(V_f/V_o)} \qquad (9)$$

Here, *a-b* is the desired velocity dependence of friction, $d\mu_{ss}$ is the change in steady-state friction resulting from the instantaneous change in velocity, and V_o and V_f are the original and final sliding velocities, respectively, which are both knowns.

Using the modelled friction path, I determine an accurate positive or negative value of the change in steady-state friction $d\mu_{ss}$ with respect to each velocity step. The net change in the modelled friction coefficient is obtained by averaging horizontal segments of friction before and after the velocity step – as shaded in red in *Figure 8* – and subtracting the initial steady-state from the resulting steady-state. Then, *a-b* is calculated by dividing the result by the natural logarithm of the velocity quotient.

6.5. Documenting pore volume changes

As shown in Equations xii-xiii in Appendix B, calibrations convert voltage measurements from a LVDT on the pore fluid piston to displacement (mm). The displacement measurements are then used to calculate pore volume changes (ml) in the gouge layer. A reference frame for pore volume is plotted with shear displacement to show occurrences of dilatancy or compaction in the sample (*Figure 10*). Measurements of volume change between imposed steps in sliding velocity are documented in conjunction with frictional behavior (see *Table 1.2*. in Appendix A). The pore volume data are smoothed with a moving average with n = 50 as the subsequence length. Compared to the friction coeffficient data, the pore volume data still contain large amounts of electronic noise even after the filtering is applied; however, the general pore volume path is still discernible.

7. Presentation of Data

Measurements of friction, pore volume, shear displacement, *a-b*, and sliding velocity are depicted in the figures below. In *Table 1.1.*, I summarize the experimental conditions and observed friction coefficient ranges in each of the tests.

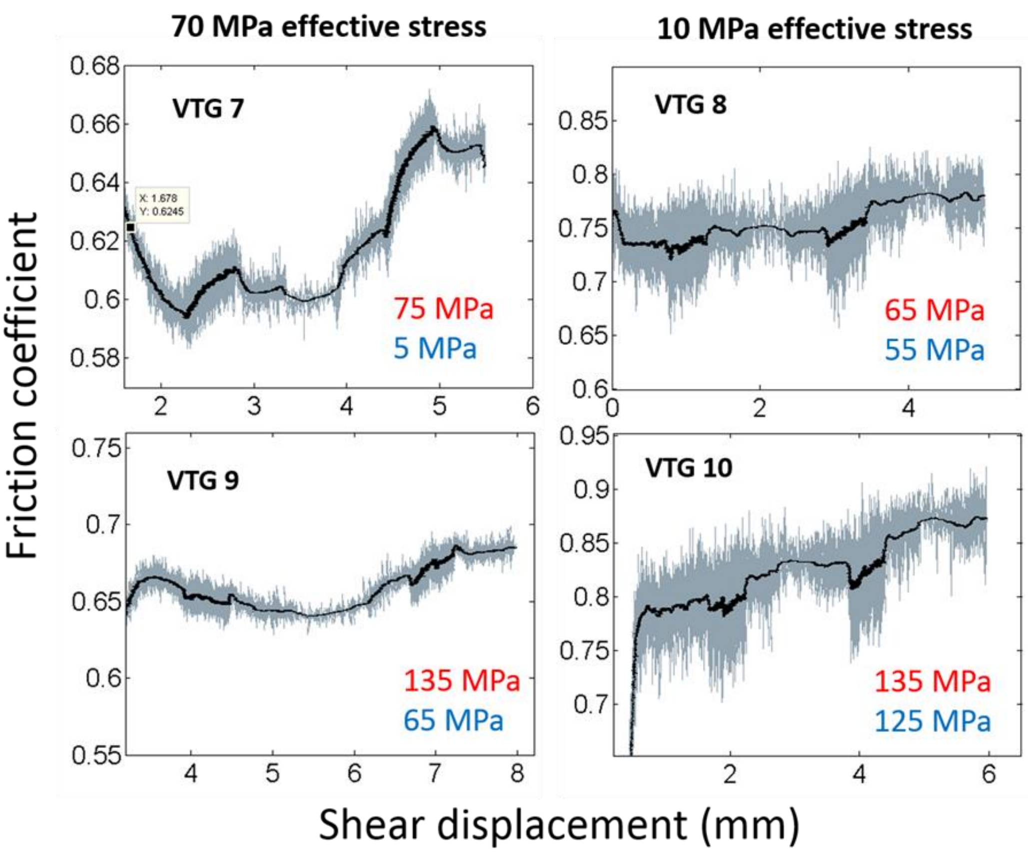

Figure 9: Measurements of the friction coefficient during each of the experiments. The friction coefficient is calculated by taking the ratio of the recorded shear and normal stress paths. The original friction data, including electronic noise in the signal, are shown in grey. The smoothed data, determined by taking a moving average (n=75) through the signal, are shown in black. The evolution of the friction coefficient with increasing strain represents strain hardening.

Table 1.1. Summary of *Figure 9*

Sample ID	Confining pressure (MPa)	Pore fluid pressure (MPa)	Effective normal stress (MPa)	Measured friction coefficient (σ_s/σ_n)
VTG 7	75	5	70	0.594 - 0.659
VTG 8	65	55	10	0.723 - 0.784
VTG 9	135	65	70	0.640 - 0.687
VTG 10	135	125	10	0.785 - 0.874

Figure 10: Changes in pore volume (ml) are plotted with shear displacement (mm). The values in the pore volume axis (~20, 30 ml) are not the absolute values of the gouge layer itself, yet they serve as a reference frame for the absolute change in volume in the gouge. General changes in pore volume are discernible in the noisy signal and are measured to document dilatancy and compaction of the sample at each velocity step.

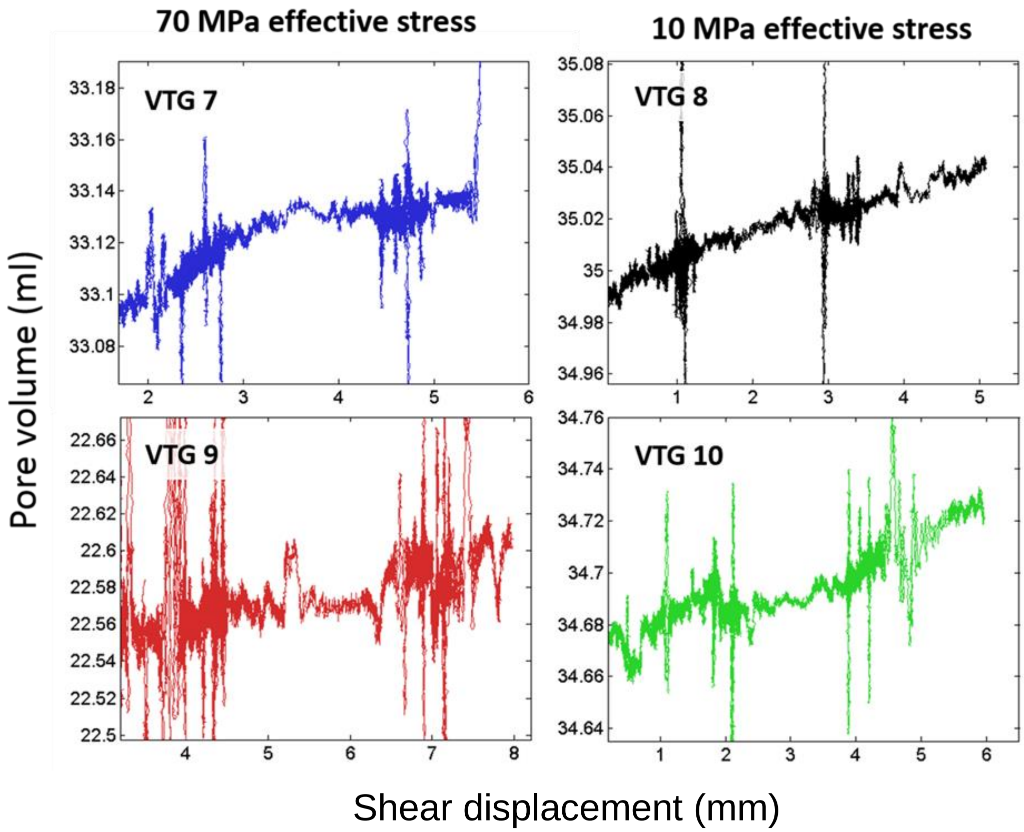

Figure 11: Calculated *a-b* values for each of the experiments are plotted with velocity to compare the frictional behavior of serpentinite at variable pore fluid pressure and effective normal stress. Positive *a-b* values are above the reference line and indicate velocity-strengthening behavior, in contrast to negative *a-b* values which are below and indicate velocity-weakening. Error bars are contained within the data points (i.e. circles), which are exaggerated in size. The filled in circles represent *a-b* determined from increases in loading velocity and the open circles designate steps decreasing in velocity.

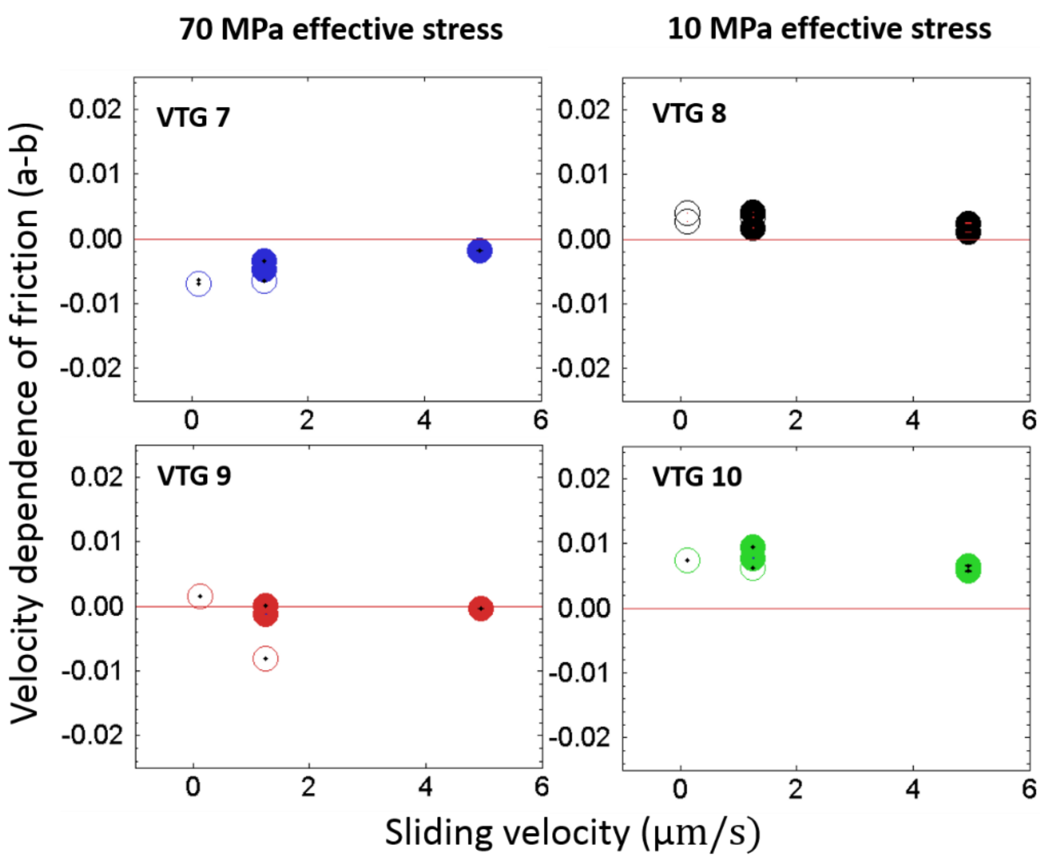

I perform two estimations of uncertainty in the frictional behavior analysis. First, I calculate the standard deviation of steady-state friction measurements at each velocity step (e.g. within the red patches in Figure 8). Second, I calculate the standard error of the mean used to average the values of steady-state friction, which I then propagate to determine a standard error in calculating the velocity-dependence of friction. The standard deviation of steady-state friction and the standard error of *a-b* at each velocity step is included in *Table 1.2*.

Twenty-five *a-b* values are calculated from the four experiments and plotted in *Figure 12* to compare frictional behavior at different pore fluid pressure, normal stress, and effective normal stress. Sample VTG10, which was sheared at the highest pore pressure and normal stress (125 and 135 MPa respectively), is shown to exhibit the largest magnitude of velocity-strengthening during the series of velocity steps. Slightly lower velocity-strengthening is exhibited by the serpentinite sheared at 55 MPa pore fluid pressure and 65 MPa normal stress (VTG8), which shows a nearly identical trend to VTG10 in decreasing *a-b* behavior with sliding velocity. The sample sheared at 65 MPa pore fluid pressure and 135 MPa normal stress (VTG9) exhibits lower *a-b* values than VTG8, including three negative data points that plot within the marginal velocity-weakening zone, and it also exhibits a decrease in *a-b* behavior with increasing velocity (with exception to one outlier). Lastly, the sample sheared at 5 MPa pore fluid pressure and 75 MPa normal stress (VTG7) velocity-weakens at each of the imposed steps; however, *a-b* increases (i.e. becomes less negative) with increasing velocity thus displaying a reverse trend compared to the other samples.

8. Discussion of Results

8.1. Velocity dependence of friction (*a-b*) results

A few interpretations can be made from *Figure 11*. First, the dichotomy in *a-b* behavior is visibly correlated with the difference in effective stress. Velocity-strengthening is the dominant frictional behavior at low effective stress (10 MPa), as shown by the locations of *a-b* in the upper half of the plot for samples VTG8 and VTG10. In contrast, velocity-weakening occurs only in the other pair of samples, VTG7 and VTG9, which were sheared at higher effective stress (70 MPa). From this, I interpret that low effective stress enhances velocity-strengthening and that high effective stress enhances velocity-weakening. Pore fluid pressure plays a key role in reducing effective normal stress (Equation 2), so another way to describe this relationship is that increasing pore fluid pressure with constant normal stress enhances frictional stability.

There is also supporting evidence that increasing pore fluid pressure while equally increasing normal stress provides yet another means to increase *a-b*. Sample VTG10 exhibits greater velocity-strengthening than that exhibited by sample VTG8 – shown more clearly in *Figure 12* below – even though both samples were strained at 10 MPa effective stress. Likewise, VTG9 exhibits a transition from marginal velocity-strengthening to marginal velocity-weakening, whereas VTG7 experiences generally greater degrees of velocity-weakening. Comparisons between these pairs indicate that magnitudes of normal stress and pore fluid pressure also influence the frictional behavior of the gouge layer, independently of effective stress. These results pose implications for slow slip mechanisms in subduction zones.

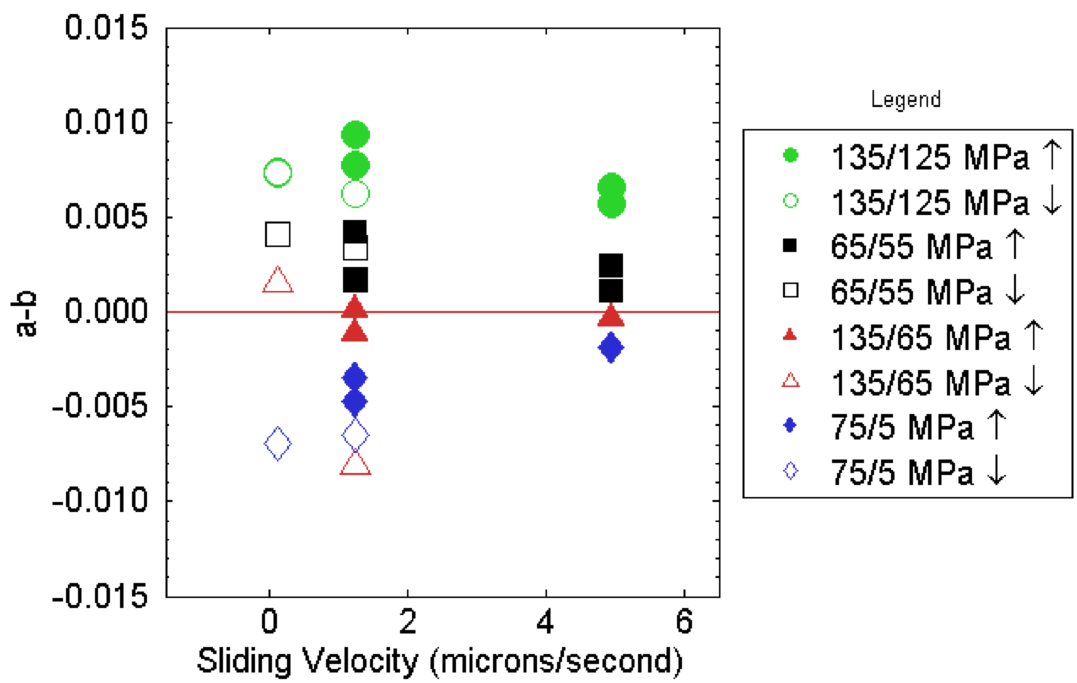

Figure 12: Data from each of the friction tests plotted separately in *Figure 11* are plotted in one window to highlight differences in frictional behavior. Results show that low effective stress increases *a-b* (as shown by the position of the green and black data points) and high effective stress decreases *a-b*. In addition, velocity-strengthening is enhanced by elevations in fluid pressure and normal stress with no change in effective stress, which alarmingly challenges the effective stress law.

8.2. Dilatancy Results

Although each of the samples are shown to dilate during deformation, the magnitudes of dilatancy differ with imposed pore fluid pressure and effective stress. The highest magnitude of dilatancy occurs in sample VTG8 and is observed by a pore volume increase of approximately 0.038 ml between the first and last velocity steps. The second highest magnitude of dilatancy occurs in sample VTG10 which is documented to expand by approximately 0.030 ml. Samples VTG7 and VTG9 expand in total by approximately 0.026 ml and 0.028 ml, respectively. The differences in pore volume change between these experiments seem to indicate that the serpentinite gouge dilates with shear more readily at low effective stress and low confining pressure and pore fluid pressure. However, relatively poor resolution of the pore volume data renders notable uncertainty (see Appendix A, *Table 1.2.* for measurements of incremental pore volume change and their standard deviations).

In addition to magnitude, the duration and initiation of dilatancy are shown to be unique for individual tests. For the most part, sample VTG8 dilates constantly with displacement; however, small perturbations occur at velocity steps transitioning out of or into peak velocity. The largest instantaneous change in pore volume occurs in response to the seventh velocity step, which marks the second transition from 1.2 x 10^{-6} m/s to 4.9 x 10^{-6} m/s. At this step, pore volume expands almost instantaneously by ~0.015 ml, after which, it compacts transiently to its prior state and then begins to dilate again. In comparison, evolution of pore volume within the other three samples is not as constant overall. The pore volume of sample VTG10 for example increases at different rates. First its pore volume increases constantly with displacement until the first peak velocity is reached. Then another response occurs in which the pore volume dilates slightly before compacting, in this case, to a lower volume than what was previously held. The sample then resumes dilation, though slower than it did previously, until again dilating faster by the sixth velocity step. As an aside, it is interesting to note that perturbations in the pore volume data after steps one and five appear to be associated with the irregular jaggedness of the evolutionary effects in the friction data. More examples of unique pore volume behavior are also exhibited by sample VTG7. The sample gradually accommodates most of its dilatancy by the fourth step and then maintains generally constant pore volume for the rest of the test. Also, between the third and fourth step, there is a curve in the sample's pore volume path representing a transition from dilatancy to compaction. This hyperbola appears to inversely reflect the observed evolutionary decay and subsequent strain hardening in the friction data. Finally, unlike the aforementioned samples, sample VTG9 dilates almost entirely within just one velocity step. Note the pore volume of

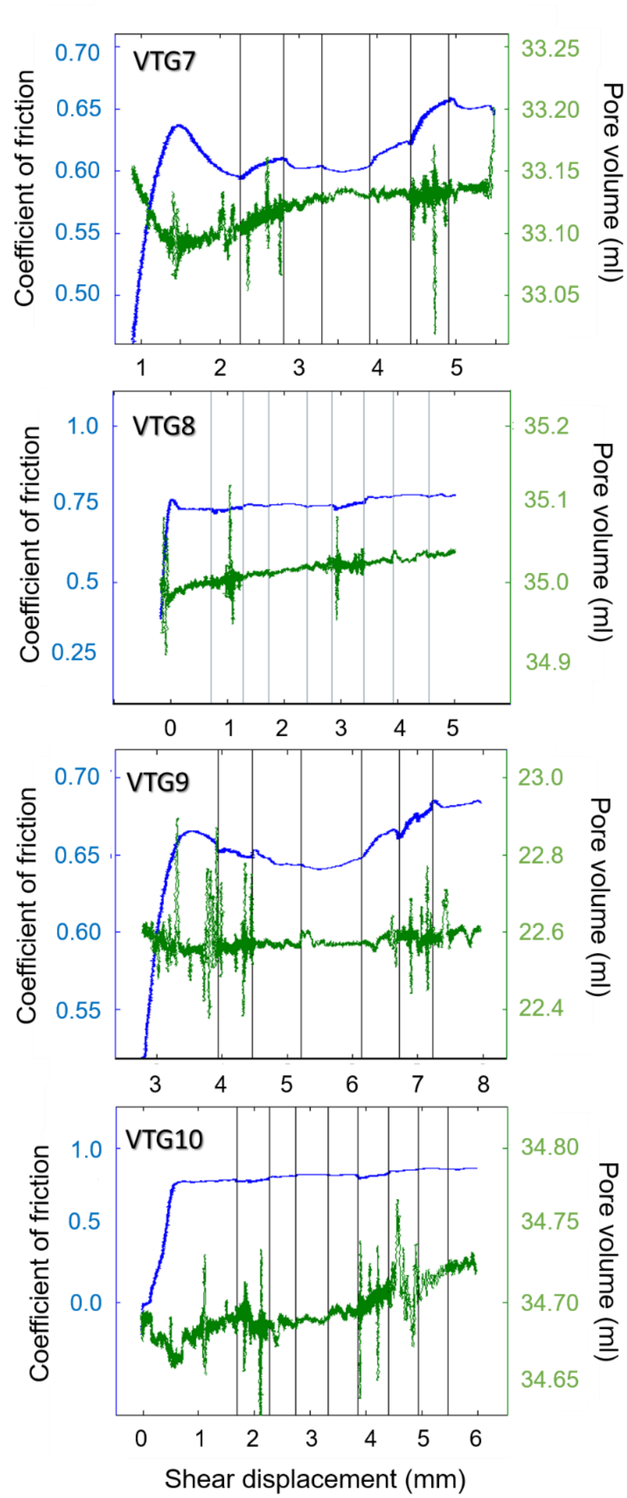

Figure 13. Pore volume changes are compared with frictional responses between velocity steps to determine if dilatancy or compaction occurs in conjunction with frictional sliding processes. The vertical lines signify the sudden changes in sliding velocity.

sample VTG9 does not expand permanently until the fourth velocity step which marks the first and only downwards transition out of peak velocity. In response to this velocity step, the pore volume initially compacts with shear and then dilates to a higher magnitude which is mostly held constant for the remainder of the experiment. Evidence that pronounced dilation occurs while *a-b* decreases dramatically (*Figure 13*) and while the rate of strain hardening increases seems to support dilatant hardening as a possible back-stop for velocity-weakening.

9. Conclusions and Broader Implications

Results of this study offer implications for slow slip behavior in subduction zones. Friction tests that impose different magnitudes of pore fluid pressure and constant confining pressure reveal that high effective stress favors velocity-weakening whereas low effective stress favors velocity-strengthening. This relationship supports that heterogeneities of fluid pressure within slow slip regions along the subducting plate interface could control variations in slip activity. Lower-fluid-pressure zones could increase potential for frictional instability on faults and cause enough unstable acceleration to produce low, non-volcanic tremor. Higher fluid pressures, conversely, could stabilize slow slip. The dependence of frictional behavior on effective stress is relevant both along strike of the plate interface and along dip; effective stresses can vary spatially and temporally with dynamic imbalances of fluid pressure and lithostatic stress.

Frictional behavior comparisons between experiments also indicate that velocity-strengthening is enhanced by elevations in fluid pressure and confining pressure with no change in effective stress. This could imply that slow slip stabilizes with depth if the rise in fluid pressure matches that of the lithostatic stress to maintain effective pressure (e.g. a slow slipping fault subjected to 10 MPa effective stress at 40 km depth could exhibit greater frictional stability than an identical fault subjected to 10 MPa effective stress at 30 km depth). If with increasing depth, however, the increase in pore fluid pressure does not keep up with the increase in lithostatic stress, then the elevation in effective stress could outcompete that of fluid pressure and transitionally induce velocity-weakening.

Changes in frictional behavior between experiments of equal effective stress disobeys the effective stress law. 125 MPa pore fluid pressure is only but an eighth of the in situ fluid pressures predicted at slow slip depths yet still significantly higher than pressures tested in other experimental studies. As such, no evidence has been documented of frictional behavior changing with pore fluid pressure and normal stress, independently of effective stress, until now. The present study reveals challenges in using the effective stress law to extrapolate frictional behavior at in situ pressures deep in the Earth's crust.

10. Suggestions for Future Work

Future work can be achieved to better explain mechanisms underlying the variable frictional behavior presented in this study and to improve analyses of frictional sliding processes. For example, improved resolution of the pore volume measurements could further reveal mechanical changes that might have influenced variations in *a-b*, including those between experiments of equal effective stress. Descriptive thin section analyses of deformed and non-deformed samples could also show evidence of dilatancy and characterize the constitution and fabric of the gouge via point counts and orientation measurements, which could provide insight into the mechanical behavior. Lastly, further analysis of the corrected friction data could include measuring the critical slip distance, D_c, between velocity steps to obtain constitutive parameters other than *a-b*.

Additional experiments can be conducted to strengthen interpretations of the present *a-b* data. For example, constant displacement tests could determine a function between displacement and the rate of strain hardening on the gouge. The function would be used to apply a nonlinear correction to the original friction coefficient path, which might better remove the effects of strain hardening than the current system which corrects multiple linear segments, individually. In addition, interpretations of how pore fluid pressure and confining pressure influence *a-b* independently of effective stress are limited, in part, because imposed fluid pressures between experiments VTG8 and VTG9 are unequal. Note this was not originally intended; both experiments were meant to impose 65 MPa. However, experiment VTG8 utilized a former pore pressure transducer which was unable to maintain pressure at 65 MPa during loading. As such, confining pressure and pore fluid pressure were lowered to 65 and 55 MPa, respectively, to maintain low effective stress and continue the experiment. By using the newly added pore pressure transducer, however, I could reattempt this friction test at 75 MPa confining pressure and 65 MPa fluid pressure to reveal more information on how fluid pressure, confining pressure, and effective stress dependently and independently influence frictional behavior.

The present study provides baseline evidence of the effects of fluid pressure and effective stress on serpentinite gouge at room-temperature. Subduction zone systems where slow slip occurs are far more complex. To understand how other conditions and processes in subduction zones affect the frictional behavior of serpentinite fault gouge, I could extend this study by analyzing the effects of temperature, fluid chemistry, and transient fluid pressure on the frictional behavior. Friction tests at elevated temperatures could be achieved using an external thermal coil to generate heat and argon gas as the confining fluid in the vessel of the hot-press. Chemical effects on slip behavior can also be tested by using the Autolab 1500 apparatus in the Rock Physics Lab to inject SiO_2 or CO_2 rich fluid through the sample instead of distilled water. Finally, friction tests with transient increases in pore fluid pressure during slip can be simulated by holding fluid pressure constant while reducing confining pressure.

11. Acknowledgements

I would like to thank my two advisors for their constant support in this thesis research. I am deeply grateful to Dr. Melodie French for recruiting me into the Rock Physics Lab in the summer 2015 and for her close mentorship this year. It has been an awesome opportunity to work with her, and I thank her for her comments on my thesis drafts and for all the guidance she has given me. In addition, I would like thank Dr. Wenlu Zhu for her help during the development stages of my project, for her useful advice in delivering presentations and drafting my thesis, and for her eloquent explanations of important background concepts. Along with my advisors, I wish to thank the rest of the Rock Physics Group – Harry Lisabeth, Jiangyi Hou, Tiange Xing, Will Kibikas, and Shayna Quidas – for their constructive feedback on my practice talks and for sharing and discussing peer reviewed papers each week. I would also like to express thanks to Dr. Philip Candela for reviewing my thesis draft and for permitting me to submit my proposal at the beginning of this spring semester. Because of this, I am happy to graduate on time. Finally, I thank my friends and family for their patience, love, and support.

12. Bibliography

Anderson, E. M. (1905). The dynamics of faulting. Transactions of the Edinburgh Geological Society 8.3: 387-402.

Ben-Zion, Y., and J. R. Rice (1997), Dynamic simulations of slip on a smooth fault in an elastic solid, J. Geophys. Res., 102(B8), 17771–17784, doi:10.1029/97JB01341.

Chapman, J. S., and T.I. Melbourne (2009). Future Cascadia megathrust rupture delineated by episodic tremor and slip. Geophysical Research Letters 36.22.

Chester, F. M. (1994), Effects of temperature on friction: Constitutive equations and experiments with quartz gouge, J. Geophys. Res., 99(B4),7247–7261, doi:10.1029/93JB03110.

Dieterich, J. H. (1979), Modeling of rock friction: 1. Experimental results and constitutive equations, J. Geophys. Res., 84(B5), 2161–2168, doi:10.1029/JB084iB05p02161.

Douglas, A., J. Beavan, L. Wallace, and J. Townend (2005), Slow slip on the northern Hikurangi subduction interface, New Zealand, Geophys. Res. Lett.,32, L16305, doi:10.1029/2005GL023607

Dragert, Herb, Kelin Wang, and Thomas S. James. A silent slip event on the deeper Cascadia subduction interface. *Science* 292.5521 (2001): 1525-1528.

Evans, B. et al., 1976, Stability of chrysotile and antigorite in the serpentine multisystem, Schweizerische mineralogische und petrographische Mitteillungen. 56. 79-93

Hawthorne, J. C., and A. M. Rubin (2010), Tidal modulation of slow slip in Cascadia, J. Geophys. Res., 115, B09406, doi:10.1029/2010JB007502.

Ito, Yoshihiro, et al. Episodic slow slip events in the Japan subduction zone before the 2011 Tohoku-Oki earthquake. Tectonophysics 600 (2013): 14-26.

Kodaira, S., et al. High pore fluid pressure may cause silent slip in the Nankai Trough. *Science* 304.5675 (2004): 1295-1298.

Kostoglodov, V., S. K. Singh, J. A. Santiago, S. I. Franco, K. M. Larson, A. R. Lowry, and R. Bilham (2003), A large silent earthquake in the Guerrero seismic gap, Mexico, Geophys. Res. Lett., 30, 1807, doi:10.1029/2003GL017219, 15.

Lockner, D. A., R. Summers, and J. D. Byerlee. Effects of temperature and sliding rate on frictional strength of granite. *Pure and applied geophysics*124.3 (1986): 445-469.

[Mair and Marone, 1999], temperature [Lockner et al., 1986], composition of gouge mixture [Moore and Lockner, 2011], etc.).

Mair, Karen, and Chris Marone. Friction of simulated fault gouge for a wide range of velocities and normal stresses. *J. Geophys. Res* 104.28,899 (1999): e28.

Marone, Chris, C. Barry Raleigh, and C. H. Scholz. Frictional behavior and constitutive modeling of simulated fault gouge. *J. geophys. Res* 95.B5 (1990): 7007-7025.

Miyazaki, S., P. Segall, J. J. McGuire, T. Kato, and Y. Hatanaka (2006), Spatial and temporal evolution of stress and slip rate during the 2000 Tokai slow earthquake, J. Geophys. Res., 111, B03409, doi:10.1029/2004JB003426.

Moore, D.E., and Lockner, D.A. (2011), Frictional strengths of talc-serpentine and talc-quartz mixtures, Journal of Geophysical Research. 116.

Obara, K. et al., (2004) Episodic slow slip events accompanied by non-volcanic tremors in southwest Japan subduction zone. Geophys. Res. Lett. 31.

Ohta, Y. et al, (2006) A large slow slip event and the depth of the seismogenic zone in the south central Alaska subduction zone, Earth and Planetary Science Letters Volume 247, Issues 1–2, 15 July 2006, Pages 108–116

Okazaki, K., and I. Katayama. (2015). Slow stick slip of antigorite serpentinite under hydrothermal conditions as a possible mechanism for slow earthquakes." *Geophysical Research Letters* 42.4: 1099-1104.Peacock, S. M. (2009), Thermal and metamorphic environment of subduction zone episodic tremor and slip, J. Geophys. Res., 114, B00A07, doi:10.1029/2008JB005978.

Peng, Z. and J. Gomberg (2010), An integrated perspective of the continuum between earthquakes and slow-slip phenomena, *Nature Geoscience* **3**, 599 - 607

Reinen, L. et al., 1991, The frictional behavior of serpentinite: Implications for aseismic creep on shallow crustal faults, *Geophysical Research Letters*. 18., 1921-1924.

Rogers, Garry, and Herb Dragert. Episodic tremor and slip on the Cascadia subduction zone: The chatter of silent slip. Science 300.5627 (2003): 1942-1943.

Ruina, Andy. Slip instability and state variable friction laws. *J. geophys. Res* 88.10 (1983): 359-10.

Scholz, H. (1998) Earthquakes and friction laws, *Nature* **391**, 37-42 (1 January 1998) | doi:10.1038/34097

Schwartz, Susan Y., and Juliana M. Rokosky. Slow slip events and seismic tremor at circum-Pacific subduction zones. *Reviews of Geophysics* 45.3 (2007).

Segall, P., et al., (2010). Dilatant strengthening as a mechanism for slow slip events. *Journal of Geophysical Research: Solid Earth (1978–2012)* 115.B12 (2010).

Shelly, D. R. (2009), Possible deep fault slip preceding the 2004 Parkfield earthquake, inferred from detailed observations of tectonic tremor, Geophys. Res. Lett., 36, L17318, doi:10.1029/2009GL039589.

Shelly, D. R., and K. M. Johnson (2011), Tremor reveals stress shadowing, deep postseismic creep, and depth-dependent slip recurrence on the lower-crustal San Andreas Fault near Parkfield, Geophys. Res. Lett., 38, L13312, doi:10.1029/2011GL047863.

Wicks, F. J., and E.J.W. Whittaker, Serpentine textures and serpentinization, Can. Mineral., 15, 459-488, 1977.

Whittaker, E. J. W., and J. Zussman. (1956), The characterization of serpentine minerals by X-ray diffraction. *Mineral. Mag* 31.233 107-126.

Ulmer, P., and V. Trommsdorff (1995), Serpentine stability to mantle depths and subduction-related magnetism, *Science*, 268, 858-61

Zhu, W., and T. Wong (1997), The transition from brittle faulting to cataclastic flow: Permeability evolution, J. Geophys. Res., 102(B2), 3027–3041, doi:10.1029/96JB03282

Appendix A, Table 1.2.

	VTG7	*Step*	*Displacement (mm)*	*Velocity (μm/s)*	μ_{ss} *(model)*	*S.d.* μ_{ss} ± *(sig-1)*	*a-b*	*Standard error in a-b*	Description	*Pore volume change (mL) from step n to n+1*	*S.d. pore volume change (mL)*
μ	0.594-0.659										
		0	1.79	0.530							
Pressure conditions	*(Mpa)*	1	0.54	0.121	0.5566	5.20E-04				0.016	±0.003
P_c	75	2	0.49	1.250	0.5457	1.61E-04	-0.0047	7.78E-06	v-weakening	0.006	±0.002
P_f	5	3	0.58	4.943	0.5431	4.47E-04	-0.0019	2.26E-05	v-weakening	0.005	±0.002
σ_e	70	4	0.51	1.250	0.5529	3.61E-04	-0.0071	4.01E-05	v-weakening	0	±0.003
S_f	1.2	5	0.53	0.121	0.5691	5.36E-04	-0.0069	1.49E-05	v-weakening	0.001	±0.004
		6	0.53	1.250	0.5610	3.47E-04	-0.0035	1.07E-05	v-weakening		

	VTG8	*Step*	*Displacement (mm)*	*Velocity (μm/s)*	μ_{ss} *(model)*	*S.d.* μ_{ss} *(sig-1)*	*a-b*	*Standard error in a-b*	Description	*Pore volume change (mL) from step n to n+1*	*S.d. pore volume change(mL)*
μ	0.723-0.784	0	1.03	0.530	0.7357	1.08E-03					
		1a	0.55	0.121	0.7316	2.03E-03	0.0027	3.27E-05	v-strengthening	0.007	±0.003
Pressure conditions	*(Mpa)*	1b			0.7389	1.97E-03					
P_c	65	2	0.45	1.250	0.7486	4.90E-04	0.0041	2.05E-05	v-strengthening	0.004	±0.001
P_f	55	3	0.74	4.943	0.7519	6.55E-04	0.0024	4.59E-05	v-strengthening	0.01	±0.001
σ_e	10	4	0.47	1.250	0.7473	4.45E-04	0.0034	4.29E-05	v-strengthening	0.004	±0.002
S_f	2.74	5a	0.56	0.121	0.7378	1.89E-03	0.0041	1.38E-05	v-strengthening	0.001	±0.003
		5b			0.6222	1.89E-03					
		6a	0.54	1.250	0.6261	7.62E-04	0.0017	2.26E-05	v-strengthening	0.005	±0.002
		6b			0.7721	8.89E-04					
		7a	0.62	4.943	0.7736	2.57E-04	0.0011	4.56E-05	v-strengthening	0.007	±0.001
		7b			0.7819	7.39E-04					
		8	0.50	1.250	0.7796	2.28E-03	0.0017	8.03E-05	v-strengthening		

	VTG9	*Step*	*Displacement (mm)*	*Velocity (μm/s)*	μ_{ss} *(model)*	*S.d.* μ_{ss} *(sig-1)*	*a-b*	*Standard error in a-b*	Description	*Pore volume change (mL) from step n to n+1*	*S.d. pore volume change(mL)*
μ	0.640-0.687	0	1.81	0.530							
		1	0.55	0.121	0.6728	0.0011				0.008	±0.005
Pressure conditions	*(Mpa)*	2	0.63	1.250	0.6700	6.44E-04	-0.0012	1.25E-05	v-weakening	0.001	±0.005
P_c	135	3	0.93	4.943	0.6696	1.91E-04	-0.0003	2.48E-05	v-weakening	0.001	±0.003
P_f	65	4	0.50	1.250	0.6807	3.31E-04	-0.0081	2.10E-05	v-weakening	0.023	±0.004
σ_e	70	5	0.55	0.121	0.6771	4.89E-04	0.0016	8.20E-06	v-strengthening	-0.007	±0.007
S_f	3.15	6	0.58	1.250	0.6773	2.21E-04	0.0001	5.19E-06	v-strengthening		

	VTG10	*Step*	*Displacement (mm)*	*Velocity (μm/s)*	μ_{ss} *(model)*	*S.d.* μ_{ss} *(sig-1)*	*a-b*	*Standard error in a-b*	Description	*Pore volume change (mL) from step n to n+1*	*S.d. pore volume change(mL)*
μ	0.785-0.874	0	1.65	0.530	0.6809	0.0017					
		1a	0.57	0.121	0.6701	0.0023	0.0073	3.54E-05	v-strengthening	-0.007	±0.004
Pressure conditions	*(Mpa)*	1b			0.6680	0.0032					
P_c	135	2a	0.51	0.125	0.6861	0.0014	0.0077	3.12E-05	v-strengthening	-0.001	±0.002
P_f	125	2b			0.7538	0.0016					
σ_e	10	3	0.62	4.943	0.7617	0.0007	0.0057	7.34E-05	v-strengthening	0.005	±0.001
S_f	4.15	4a	0.47	1.250	0.7531	0.0008	0.0062	6.31E-05	v-strengthening	0.005	±0.003
		4b			0.8301	0.0013					
		5	0.53	0.121	0.8126	0.0032	0.0075	2.72E-05	v-strengthening	0.012	±0.003
		6a	0.54	0.125	0.8285	0.0024	0.0068	4.06E-05	v-strengthening	0.004	±0.012
		6b			0.7704	0.0021					
		7	0.55	4.943	0.7794	0.0009	0.0065	6.12E-05	v-strengthening	0.012	±0.004

Appendix B:

Matlab script for instrument component calibrations and friction coefficient and pore volume output

Voltage measurements

i. ***M = load ('VTG_data.csv'***);
%column 1: LC raw voltage
%column 2: axial displ. raw voltage
%column 3: Pc raw voltage
%column 4: Pf LVDT
%column 5: Pc LVDT
%column 6: Pf raw voltage

Input variables measured before experiment

ii. ***d = ;*** *% length of sandstone (mm)*
iii. ***ad0= ;*** *% initial axial displacement (mm)*
iv. ***sealF = ;*** *% seal friction (MPa)*

Calibration equations

v. ***t2 = 0.5*(0:1:length(M)-1);*** *% time assuming 2 Hz recording*
vi. ***FGs = (65.343*M(:,1)+2.9339);*** *% stress on force gauge (1.5 in in diameter) (MPa)*
vii. ***ad =(7885.7*(M(:,2))+46.4)/1000-(7885.7*(M(1,2))+46.4)/1000-0.004654*(FGs-FGs(1));*** *% axial displacement from LDVT on main ram (mm)*
viii. ***sd = ad/cos(35*pi/180);*** *% shear displacement along sawcut at 35 to core axis (mm)*
ix. ***Pc = 94.905*M(:,3)+1.1294;*** *% confining pressure (MPa)*
x. ***Pf = 11.099*M(:,6)-0.3333;*** *% pore pressure (MPa) calibrated to old tranducer used in experiments VTG7 and VTG8*
xi. ***Pf_new = 21.333*M(:,6)-1.7264;*** *% pore pressure calibrated to new transducer used in experiments VTG9 and VTG10*
xii. ***Pflvdt = (9.6409*M(:,5)+103.5);*** *% displacement (mm)*
xiii. ***Pvol = (9.6409*M(:,5)+103.5)/10*(pi*((0.895*2.54)/2)^2);*** *% volume change (mL)*
xiv. ***Ds = (FGs-Pc-sealF)*2.25;*** *% differential stress on sample 1" in diameter (MPa).*
xv. ***AL = Pc+Ds;*** *% axial stress on sample (MPa)*
xvi. ***T = pi-2*asin(ad/d*tan(35*pi/180));*** *% area correction for stress on sawcut with increasing slip: part 1*
xvii. ***Af = (T-sin(T))/pi;*** *% area correction for stress on sawcut with increasing slip: part 2*
xviii. ***Dscor = Ds./Af;*** *% differential stress (MPa) on sample corrected for area*
xix. ***Ss = 0.5*(Dscor)*sin(2*35*pi/180);*** *% shear stress (MPa) on sawcut corrected for area*
xx. ***Sn = Pc-Pf+0.5*(Dscor)*(1-cos(2*35*pi/180));*** *% normal stress (MPa) on sawcut corrected for area*
xxi. ***mu = Ss./Sn;*** *% friction coefficient*

14. Scratch Matlab Code for Processing Experiments

VTG7

```
% moving average to smooth friction coefficient (n = 75)

for i = 1:75
    mus(i) = (mu(i));% mus = smoothed mu
end
for i = 76:n-75
    mus(i) = sum(mu(i-75:i+75))/151;
end
for i = n-74:n
    mus(i) = mu(i);
end

% moving average to smooth pore volume (n = 50)

for i = 1:50
    Pvols(i) = (Pvol(i));% mus = smoothed mu
end
for i = 51:n-50
    Pvols(i) = sum(Pvol(i-50:i+50))/101;
end
for i = n-49:n
    Pvols(i) = Pvol(i);
end

%
sdavg = sds';
t = t2';
T_interest = t(11728:43080);
Sd_t = sd(11728:43080,1); % time appropriate shear displacement
Ad_t = ad(11728:43080,1); % axial displacement during steps
Mu_t = mu(11728:43080,1); % frictional strength during steps
Pf_t = Pf(11728:43080,1); % frictional strength during steps

mus_i = mus';
Mus_t = mus_i(11728:43080,1); % smoothed friction by moving average

% Correct slope or add segments or both

Muc_segment1 = Mus_t(1:19973)-(0.0193.*Sd_t(1:19973));
Mu_segment2 = Mus_t(19973:20849)-(0.5987-0.5419);
Muc_segment3 = Mus_t(20849:30435)-(0.0304.*Sd_t(20849:30435))+(0.0614);
Mu_segment4 = Mus_t(30435:31353)-(0.6556-0.5727+0.0035+0.0033);

%%%%%%%%%%%%%%%%%%%%%%%%%%%

% Plot original signal and smoothed data of friction coefficient vs shear
displacement
```

```
figure(8);
plot(Sd_t(5000:31353),Mus_t(5000:31353),'k');
hold on;
plot(Sd_t(1:19973),Muc_segment1,'g');
hold on;
plot(Sd_t(19973:20849),Mu_segment2,'k');
hold on;
plot(Sd_t(20849:30435),Muc_segment3,'g');
hold on;
plot(Sd_t(30435:31353),Mu_segment4,'k');
ylim([0.525 0.665]);
xlim([1.7 5.8]);
set(gca,'fontsize',20);

figure(9);
plot(Sd_t(5000:31353),Mu_t(5000:31353),'r','Color',[.57,.64,0.69]); hold on;
% original signal
plot(Sd_t(5000:31353),Mus_t(5000:31353),'k');
% smoothed signal

% display steady state ranges that were averaged...

% Corrected friction to slope 1
plot(Sd_t(14371:19703),Muc_segment1(14371:19703),'r');
plot(Sd_t(19973:20293),Mu_segment2(1:321),'r');
plot(Sd_t(20674:20747),Mu_segment2(702:775),'r');

% Corrected friction to slope 2
plot(Sd_t(21049:21423),Muc_segment3(201:575),'r');
plot(Sd_t(26500:30384),Muc_segment3(5652:9536),'r');
plot(Sd_t(30773:30989),Mu_segment4(389:605),'r');

% plot pore volume vs displacement

figure(10);
plot(Sd_t,Pvols_t);
ylabel('Pore volume (mL)'); xlabel('Shear displacement (mm)');
hold on;

% reference lines for V-steps
plot([2.262 2.262],[33.06 33.22],'r');
plot([2.805 2.805],[33.06 33.22],'r');
plot([3.337 3.337],[33.06 33.22],'g');
plot([3.904 3.904],[33.06 33.22],'g');
plot([4.421 4.421],[33.06 33.22],'r');
plot([4.910 4.910],[33.06 33.22],'r');


%% Plot a-b

% Change in sliding velocity
```

```
V1=0.5299294;
V2=0.1211172;
V3=1.2499073;
V4=4.9425499;
V5=1.2499073;
V6=0.1211172;
V7=1.2499073;
V8=4.9425499;
V9=1.2499073;

% Average of steady state friction

mu1 = mean(Muc_segment1(14371:19703));
mu2 = mean(Mu_segment2(1:321));
mu3 = mean(Mu_segment2(702:775));
mu4 = mean(Muc_segment3(201:575));
mu5 = mean(Muc_segment3(5652:9536));
mu6 = mean(Mu_segment4(389:605));

% STDEV of steady state friction

std1 = std(Muc_segment1(14371:19703));
std2 = std(Mu_segment2(1:321));
std3 = std(Mu_segment2(702:775));
std4 = std(Muc_segment3(201:575));
std5 = std(Muc_segment3(5652:9536));
std6 = std(Mu_segment4(389:605));

% Length of steady state friction

lengthMu1 = length(Muc_segment1(14371:19703));
lengthMu2 = length(Mu_segment2(1:321));
lengthMu3 = length(Mu_segment2(702:775));
lengthMu4 = length(Muc_segment3(201:575));
lengthMu5 = length(Muc_segment3(5652:9536));
lengthMu6 = length(Mu_segment4(389:605));

% Diff in average coefficient of friction spanning before/after v-step

dmu1 = NaN;
dmu2 = mu2-mu1;
dmu3 = mu3-mu2;
dmu4 = mu4-mu3;
dmu5 = mu5-mu4;
dmu6 = mu6-mu5;

% standard error of mean at each steady state
sem1 = std1/sqrt(lengthMu1);
sem2 = std2/sqrt(lengthMu2);
sem3 = std3/sqrt(lengthMu3);
sem4 = std4/sqrt(lengthMu4);
sem5 = std5/sqrt(lengthMu5);
sem6 = std6/sqrt(lengthMu6);
```

```
% error propagation of dmu calculation: take square root of sum of squares
% of sem...then divide by exact value log(V2/V1)

error2=abs((sqrt(sem2^2+sem1^2))/(log(V2/V1)));
error3=abs((sqrt(sem3^2+sem2^2))/(log(V3/V2)));
error4=abs((sqrt(sem4^2+sem3^2))/(log(V4/V3)));
error5=abs((sqrt(sem5^2+sem4^2))/(log(V5/V4)));
error6=abs((sqrt(sem6^2+sem5^2))/(log(V6/V5)));


% a-b = duss/dln(V)
% ab1 = dmu1/(log(V2/V1));
ab2 = dmu2/(log(V3/V2));
ab3 = dmu3/(log(V4/V3));
ab4 = dmu4/(log(V5/V4));
ab5 = dmu5/(log(V6/V5));
ab6 = dmu6/(log(V7/V6));
% a_b = [NaN ab1 ab2 ab3 ab4 ab5 ab6];
% SV = [V1 V2 V3 V4 V5 V6 V7];

a_b_up = [ab2 ab3 ab6];
SV_up = [V3 V4 V7];
a_b_down = [NaN ab4 ab5];
SV_down = [V2 V5 V6];

figure(8);
p1 = scatter(SV_up,a_b_up,'b','filled');
p1Children = get(p1, 'Children');
set(p1Children, 'Markersize', 20);
hold on;
p2 = scatter(SV_down,a_b_down,'b');
p2Children = get(p2, 'Children');
set(p2Children, 'Markersize', 20);
set(gca,'fontsize',22);
plot([-1 6],[0 0],'r');
xlim([-1 6]);
ylim([-.025 .025]);
%ylabel('a-b'); xlabel('velocity (microns/second)');
%title('70 MPa effective pressure, 5 MPa pore pressure');
n=get(gca,'ytick');
set(gca,'yticklabel',sprintf('%.2f |',n'),'YMinorTick','on');
box on;
%title('Velocity dependence of friction at 75:5 MPa (Pc:Pf)');

%error bars

errorbar(V3,ab2,error2),'.k';
errorbar(V4,ab3,error3,'.k');
errorbar(V5,ab4,error4,'.k');
errorbar(V6,ab5,error5,'.k');
errorbar(V7,ab6,error6,'.k');
```

```
% tex1 = text(V2,ab1,'   1'); set(tex1,'Fontsize',16);
% tex2 = text(V3,ab2,'   2'); set(tex2,'Fontsize',16);
% tex3 = text(V4,ab3,'   3'); set(tex3,'Fontsize',16);
% tex4 = text(V5,ab4,'   4'); set(tex4,'Fontsize',16);
% tex5 = text(V6,ab5,'   5'); set(tex5,'Fontsize',16);
% tex6 = text(V7,ab6,'   6'); set(tex6,'Fontsize',16);


%%  Dilatancy vs friction
figure(13);
plotyy(Sd_t(5000:31353),Mus_t(5000:31353),Sd_t(5000:31353),Pvols_t(5000:31353
),'plot');
[hAx,hLine1,hLine2] =
plotyy(Sd_t(5000:31353),Mus_t(5000:31353),Sd_t(5000:31353),Pvols_t(5000:31353
));
set(gca,'fontsize',15);
title('VTG 7: Frictional behavior and Pore volume change','fontsize',15);
%xlabel('Shear Displacement (mm)','fontsize',15);
box on;
ylabel(hAx(1),'Coefficient of friction  \mu','fontsize',15,'color','k'); %
left y-axis
ylabel(hAx(2),'Pore volume (mL)','fontsize',12,'color','k'); % right y-axis


% reference lines for V-steps
hold on;
plot([2.262 2.262],[-.5 2],'r','Color',[.57,.64,0.69]);
hold on;
plot([2.805 2.805],[-.5 2],'r','Color',[.57,.64,0.69]);
hold on;
plot([3.29 3.29],[-.5 2],'r','Color',[.57,.64,0.69]);
hold on;
plot([3.904 3.904],[-.5 2],'r','Color',[.57,.64,0.69]);
hold on;
plot([4.421 4.421],[-.5 2],'r','Color',[.57,.64,0.69]);
hold on;
plot([4.910 4.910],[-.5 2],'r','Color',[.57,.64,0.69]);
```

VTG 8

```
% moving average to smooth friction coefficient (n = 75)

for i = 1:75
    mus(i) = (mu(i));% mus = smoothed mu
end
for i = 76:n-75
    mus(i) = sum(mu(i-75:i+75))/151;
end
for i = n-74:n
    mus(i) = mu(i);
end
```

```
% moving average to smooth pore volume (n = 50)

for i = 1:50
    Pvols(i) = (Pvol(i));% mus = smoothed mu
end
for i = 51:n-50
    Pvols(i) = sum(Pvol(i-50:i+50))/101;
end
for i = n-49:n
    Pvols(i) = Pvol(i);
end


T_interest = t(23180:48920);
Sd_t = sd(23180:48920,1); % time appropriate shear displacement
Ad_t = ad(23180:48920,1); % axial displacement during steps
Mu_t = mu(23180:48920,1); % frictional strength during steps
Pf_t = Pf(23180:48920,1);
Pvols_i = Pvols'; % inverse of smoothed P volume
Pvols_t = Pvols_i(23180:48920,1); % smoothed P volume over velocity steps
mus_i = mus';
Mus_t = mus_i(23180:48920,1); % smoothed friction by moving average
%y=medfilt1(Mu_t,10); % smoothed friction by median filter

% Correct slope

Mu_c = Mus_t-(((0.7764-0.761)/(3.381-2.996)).*Sd_t); %+(0.2495-0.241);
Muc_segment1 = Mu_c(16379:25600)+(0.7583-0.6427);
Mu_segment2 = (0.776-0.7292)+Mus_t-(((0.7826-0.7794)/(4.238-3.995)).*Sd_t);
%Mu_c2 = Mus_t-(((0.2461-0.238)/(2.189-1.756)).*Sd_t)+(0.2424-0.2297);

%%%%%%%%%%%%%%%%%%%%%%%%%%%

% Plot friction coefficient vs shear displacement

figure(9);
plot(Sd_t(500:25600),Mu_t(500:25600), 'r','Color',[.57,.64,0.69]);
hold on;
plot(Sd_t(500:25600),Mus_t(500:25600),'k');
hold on;

%SHOW AVERAGES
% display friction ranges that were averaged...

% Original friction
plot(Sd_t(2226:3984),Mus_t(2226:3984),'r');
plot(Sd_t(5498:7973),Mus_t(5498:7973),'r');
plot(Sd_t(10073:13000),Mus_t(10073:13000),'r');
plot(Sd_t(13374:13620),Mus_t(13374:13620),'r');
plot(Sd_t(13964:14105),Mus_t(13964:14105),'r');
plot(Sd_t(14430:14864),Mus_t(14430:14864),'r');
plot(Sd_t(24598:24734),Mus_t(24598:24734),'r');
```

```
plot(Sd_t(24973:25605),Mus_t(24973:25605),'r');

% Corrected friction to slope 1
plot(Sd_t(16379:22456),Mu_c(16379:22456),'c');
plot(Sd_t(23986:24250),Mu_c(23986:24250),'c');

% Corrected friction segment 1
plot(Sd_t(16379:22456),Muc_segment1(1:6078),'m');

% Corrected friction segment 2
plot(Sd_t(24016:24250),Mu_segment2(24016:24250),'b');
plot(Sd_t(24568:24684),Mu_segment2(24568:24684),'b');

% plot pore volume vs displacement
figure(25);
plot(Sd_t,Pvols_t);
hold on;

% reference lines for V-steps
plot([0.7216 0.7216],[34.97 35.05],'r');
plot([1.275 1.275],[34.97 35.05],'r');
plot([1.738 1.738],[34.97 35.05],'g');
plot([2.412 2.412],[34.97 35.05],'g');
plot([2.846 2.846],[34.97 35.05],'r');
plot([3.418 3.418],[34.97 35.05],'r');
plot([3.933 3.933],[34.97 35.05],'g');
plot([4.564 4.564],[34.97 35.05],'g');


%% Plot a-b

% Change in sliding velocity

V1=0.5299294;
V2=0.1211172;
V3=1.2499073;
V4=4.9425499;
V5=1.2499073;
V6=0.1211172;
V7=1.2499073;
V8=4.9425499;
V9=1.2499073;

% plot(Sd_t(24568:24684),Mu_segment2(24568:24684),'b');
% plot(Sd_t(24598:24734),Mus_t(24598:24734),'y');
% plot(Sd_t(24973:25605),Mus_t(24973:25605),'y');

% Average of steady state friction

% a & bs account for same steady state friction but at different reference
values
mu1 = mean(Mus_t(2226:3984));
```

```
mu2a = mean(Mus_t(5498:7973));
mu2b = mean(Mus_t(10073:13000));
mu3 = mean(Mus_t(13374:13620));
mu4 = mean(Mus_t(13964:14105));
mu5 = mean(Mus_t(14430:14864));
mu6a = mean(Muc_segment1(1:6078));
mu6b = mean(Mu_c(16379:22456));
mu7a = mean(Mu_c(23986:24250));
mu7b = mean(Mu_segment2(24016:24250));
mu8a = mean(Mu_segment2(24568:24684));
mu8b = mean(Mus_t(24598:24734));
mu9 = mean(Mus_t(24973:25605));

% STDEV of steady state friction

std1 = std(Mus_t(2226:3984));
std2a = std(Mus_t(5498:7973));
std2b = std(Mus_t(10073:13000));
std3 = std(Mus_t(13374:13620));
std4 = std(Mus_t(13964:14105));
std5 = std(Mus_t(14430:14864));
std6a = std(Muc_segment1(1:6078));
std6b = std(Mu_c(16379:22456));
std7a = std(Mu_c(23986:24250));
std7b = std(Mu_segment2(24016:24250));
std8a = std(Mu_segment2(24568:24684));
std8b = std(Mus_t(24598:24734));
std9 = std(Mus_t(24973:25605));

% Length of steady state friction

lengthMu1 = length(Mus_t(2226:3984));
lengthMu2a = length(Mus_t(5498:7973));
lengthMu2b = length(Mus_t(10073:13000));
lengthMu3 = length(Mus_t(13374:13620));
lengthMu4 = length(Mus_t(13964:14105));
lengthMu5 = length(Mus_t(14430:14864));
lengthMu6a = length(Muc_segment1(1:6078));
lengthMu6b = length(Mu_c(16379:22456));
lengthMu7a = length(Mu_c(23986:24250));
lengthMu7b = length(Mu_segment2(24016:24250));
lengthMu8a = length(Mu_segment2(24568:24684));
lengthMu8b = length(Mus_t(24598:24734));
lengthMu9 = length(Mus_t(24973:25605));

% Diff in average coefficient of friction spanning before/after v-step
dmu1 = mu2a-mu1;
dmu2 = mu3-mu2b;
dmu3 = mu4-mu3;
dmu4 = mu5-mu4;
dmu5 = mu6a-mu5;
dmu6 = mu7a-mu6b;
dmu7 = mu8a-mu7b;
```

```
dmu8 = mu9-mu8b;

% standard error of mean at each steady state
sem1 = std1/sqrt(lengthMu1);
sem2a = std2a/sqrt(lengthMu2a);
sem2b = std2b/sqrt(lengthMu2b);
sem3 = std3/sqrt(lengthMu3);
sem4 = std4/sqrt(lengthMu4);
sem5 = std5/sqrt(lengthMu5);
sem6a = std6a/sqrt(lengthMu6a);
sem6b = std6b/sqrt(lengthMu6b);
sem7a = std7a/sqrt(lengthMu7a);
sem7b = std7b/sqrt(lengthMu7b);
sem8a = std8a/sqrt(lengthMu8a);
sem8b = std8b/sqrt(lengthMu8b);
sem9 = std9/sqrt(lengthMu9);

% error propagation of dmu calculation: take square root of sum of squares
% of sem...then divide by exact value log(V2/V1)

error1=(sqrt(sem2a^2+sem1^2))/(log(V2/V1));
error2=(sqrt(sem3^2+sem2b^2))/(log(V3/V2));
error3=(sqrt(sem4^2+sem3^2))/(log(V4/V3));
error4=(sqrt(sem5^2+sem4^2))/(log(V5/V4));
error5=(sqrt(sem6a^2+sem5^2))/(log(V6/V5));
error6=(sqrt(sem7a^2+sem6b^2))/(log(V7/V6));
error7=(sqrt(sem8a^2+sem7b^2))/(log(V8/V7));
error8=(sqrt(sem9^2+sem8b^2))/(log(V9/V8));

% a-b = duss/dln(V)
ab1 = dmu1/(log(V2/V1));
ab2 = dmu2/(log(V3/V2));
ab3 = dmu3/(log(V4/V3));
ab4 = dmu4/(log(V5/V4));
ab5 = dmu5/(log(V6/V5));
ab6 = dmu6/(log(V7/V6));
ab7 = dmu7/(log(V8/V7));
ab8 = dmu8/(log(V9/V8));

a_b = [NaN ab1 ab2 ab3 ab4 ab5 ab6 ab7 ab8];
SV = [V1 V2 V3 V4 V5 V6 V7];

a_b_up = [ab2 ab3 ab6 ab7];
SV_up = [V3 V4 V7 V8];
a_b_down = [NaN ab1 ab4 ab5 ab8];
SV_down = [V1 V2 V5 V6 V9];

a_b_up = [ab2 ab3 ab6 ab7];
SV_up = [V3 V4 V7 V8];
a_b_down = [NaN ab1 ab4 ab5 ab8];
SV_down = [V1 V2 V5 V6 V9];

figure(6);
```

```
p1 = scatter(SV_up,a_b_up,'k','filled');
p1Children = get(p1, 'Children');
set(p1Children, 'Markersize', 20);
hold on;
p2 = scatter(SV_down,a_b_down,'k');
p2Children = get(p2, 'Children');
set(p2Children, 'Markersize', 20);
set(gca,'fontsize',22);
hold on;
plot([-1 6],[0 0],'r');
% xlim([0 1.8]);
xlim([-1 6]);
ylim([-.025 .025]);
box on;
%ylabel('a-b'); xlabel('velocity (microns/second)');
%title('10 MPa effective pressure, 55 MPa pore pressure');
%title('Velocity dependence of friction at 65:55 MPa (Pc:Pf)');
n=get(gca,'ytick');
set(gca,'yticklabel',sprintf('%.2f |',n'),'YMinorTick','on');

%error bars
errorbar(V2,ab1,error1,'r');
errorbar(V3,ab2,error2,'r');
errorbar(V4,ab3,error3,'r');
errorbar(V5,ab4,error4,'r');
errorbar(V6,ab5,error5,'r');
errorbar(V7,ab6,error6,'r');
errorbar(V8,ab7,error7,'r');
errorbar(V9,ab8,error8,'r');

tex1 = text(V2,ab1,'  1'); set(tex1,'Fontsize',16);
tex2 = text(V3,ab2,'  2'); set(tex2,'Fontsize',16);
tex3 = text(V4,ab3,'  3'); set(tex3,'Fontsize',16);
tex4 = text(V5,ab4,'  4'); set(tex4,'Fontsize',16);
tex5 = text(V6,ab5,'  5'); set(tex5,'Fontsize',16);
tex6 = text(V7,ab6,'  6'); set(tex6,'Fontsize',16);
tex7 = text(V8,ab7,'  7'); set(tex7,'Fontsize',16);
tex8 = text(V9,ab8,'  8'); set(tex8,'Fontsize',16);


figure(13);
plotyy(Sd_t(500:25600),Mus_t(500:25600),Sd_t(500:25600),Pvols_t(500:25600),'p
lot');
[hAx,hLine1,hLine2] =
plotyy(Sd_t(500:25600),Mus_t(500:25600),Sd_t(500:25600),Pvols_t(500:25600));

title('VTG 8: Frictional behavior and Pore volume change','fontsize',15);
xlabel('Shear Displacement (mm)','fontsize',15);
box on;

ylabel(hAx(1),'Coefficient of friction  \mu','fontsize',15,'color','k'); %
left y-axis
ylabel(hAx(2),'Pore volume (mL)','fontsize',15,'color','k'); % right y-axis
```

```
% reference lines for V-steps
hold on;
plot([0.7216 0.7216],[0 2],'r','Color',[.57,.64,0.69]);
hold on;
plot([1.275 1.275],[0 2],'r','Color',[.57,.64,0.69]);
hold on;
plot([1.738 1.738],[0 2],'r','Color',[.57,.64,0.69]);
hold on;
plot([2.412 2.412],[0 2],'r','Color',[.57,.64,0.69]);
hold on;
plot([2.846 2.846],[0 2],'r','Color',[.57,.64,0.69]);
hold on;
plot([3.418 3.418],[0 2],'r','Color',[.57,.64,0.69]);
hold on;
plot([3.933 3.933],[0 2],'r','Color',[.57,.64,0.69]);
hold on;
plot([4.564 4.564],[0 2],'r','Color',[.57,.64,0.69]);
```

VTG 9

```
% moving average to smooth friction coefficient (n = 75)

for i = 1:75
    mus(i) = (mu(i));% mus = smoothed mu
end
for i = 76:n-75
    mus(i) = sum(mu(i-75:i+75))/151;
end
for i = n-74:n
    mus(i) = mu(i);
end

% moving average to smooth pore volume (n = 50)

for i = 1:50
    Pvols(i) = (Pvol(i));% mus = smoothed mu
end
for i = 51:n-50
    Pvols(i) = sum(Pvol(i-50:i+50))/101;
end
for i = n-49:n
    Pvols(i) = Pvol(i);
end


T_interest = t(11728:47950);
Sd_t = sd(11728:47950,1); % time appropriate shear displacement
Ad_t = ad(11728:47950,1); % axial displacement during steps
Mu_t = mu(11728:47950,1); % frictional strength during steps
```

```
Pf_t = Pf(11728:47950,1);
Pvols_i = Pvols'; % inverse of smoothed P volume
Pvols_t = Pvols_i(11728:47950,1); % smoothed P volume over velocity steps
Pflvdt_t = Pflvdt(11728:47950,1); % smoothed P volume over velocity steps
mus_i = mus';
Mus_t = mus_i(11728:47950,1); % smoothed friction by moving average
rate = Sd_t./T_interest;

% Correct slope
Mu_c = Mus_t-(((0.6555-0.6564)/(4.450-4.277)).*Sd_t);
oops = Mus_t-(((0.6557-0.6482)/(6.62-5.601)).*Sd_t);
Muc_segment2 = (0.0911)+oops(25143:36150)-(((0.6103-0.6068)/(6.549-
5.607)).*Sd_t(25143:36150));
Muc_segment3 = 0.0387+Muc_segment2(247:11007)-(((0.6911-0.69)/(6.622-
6.448)).*Sd_t(25390:36150));
Muc_segment4 = 0.0829+Muc_segment3-(((0.691-0.6886)/(7.202-
7.01)).*Sd_t(25390:36150));
Muc_segment5 = -.1699+Muc_segment4-(((0.6694-0.6767)/(7.82-
7.511)).*Sd_t(25390:36150));



%%%%%%%%%%%%%%%%%%%%%%%%%%%

% Plot friction coefficient vs shear displacement

%plot(Sd_t(10000:36150),Mu_t(10000:36150),'r','Color',[.57,.64,0.69]);
%hold on;
plot(Sd_t(10000:36150),Mus_t(10000:36150),'k');
hold on;
plot(Sd_t(10000:36150),Mu_c(10000:36150),'g');
hold on;
plot(Sd_t(25143:25390),Muc_segment2(1:248),'b');
hold on;
plot(Sd_t(25391:26161),Muc_segment3(1:771),'k');
hold on;
plot(Sd_t(26162:34860),Muc_segment4(772:9470),'b');
hold on;
plot(Sd_t(34861:36150),Muc_segment5(9471:10760),'k');
%title('135 MPa effective pressure, 65 MPa pore pressure');
%ylabel('Friction coefficient'); xlabel('Shear displacement (mm)');
set(gca,'fontsize',20);
whitebg('w');
xlim([3.2 8.2]);
ylim([0.55 0.76]);

%friction coefficient values: 0.6414-0.6868


%SHOW AVERAGES
% display friction ranges that were corrected

hold on;
%plot(Sd_t(14421:15040),Mu_c(14421:15040),'r');
```

```
plot(Sd_t(18018:23550),Mu_c(18018:23550),'r');
hold on;
plot(Sd_t(24184:24844),Mu_c(24184:24844),'r');
hold on;
plot(Sd_t(25073:25140),Mu_c(25073:25140),'r');
hold on;
plot(Sd_t(25791:26161),Muc_segment3(401:771),'r');
hold on;
plot(Sd_t(31462:34860),Muc_segment4(6072:9470),'r');
hold on;
plot(Sd_t(35261:35900),Muc_segment5(9871:10510),'r');



figure(10);
plot(Sd_t,Pvols_t);
ylabel('Pore volume (ml)'); xlabel('Shear displacement mm');
hold on;

% reference lines for V-steps

plot([3.943 3.943],[22.5 22.75],'r');
plot([4.463 4.463],[22.5 22.75],'r');
plot([5.208 5.208],[22.5 22.75],'g');
plot([6.14 6.14],[22.5 22.75],'g');
plot([6.728 6.728],[22.5 22.75],'r');
plot([7.236 7.236],[22.5 22.75],'r');
hold off;

%% Plot a-b

% Change in sliding velocity
% V2=0.08;
V1=0.5299294;
V2=0.1211172;
V3=1.2499073;
V4=4.9425499;
V5=1.2499073;
V6=0.1211172;
V7=1.2499073;
V8=4.9425499;
V9=1.2499073;


% Average of steady state friction

mu1 = mean(Mu_c(18018:23550));
mu2 = mean(Mu_c(24184:24844));
mu3 = mean(Mu_c(25073:25140));
mu4 = mean(Muc_segment3(401:771));
mu5 = mean(Muc_segment4(6072:9470));
mu6 = mean(Muc_segment5(9871:10510));
```

```
% STDEV of steady state friction

std1 = std(Mu_c(18018:23550));
std2 = std(Mu_c(24184:24844));
std3 = std(Mu_c(25073:25140));
std4 = std(Muc_segment3(401:771));
std5 = std(Muc_segment4(6072:9470));
std6 = std(Muc_segment5(9871:10510));

% Diff in average coefficient of friction spanning before/after v-step
%dmu1 = mean(Mus_t(16518:23550))-mean(Mus_t(14421:15040));
dmu2 = mean(Mu_c(24184:24844))-mean(Mu_c(18018:23550));
dmu3 = mean(Mu_c(25073:25140)-mean(Mu_c(24184:24844)));
dmu4 = mean(Muc_segment3(401:771))-mean(Mu_c(25073:25140));
dmu5 = mean(Muc_segment4(6072:9470))-mean(Muc_segment3(401:771));
dmu6 = mean(Muc_segment5(9871:10510))-mean(Muc_segment4(6072:9470));


% standard error of mean at each steady state
sem2 = std((Mu_c(18018:23550)))/sqrt(length(Mu_c(18018:23550)));
sem3 = std((Mu_c(24184:24844)))/sqrt(length(Mu_c(24184:24844)));
sem4 = std((Mu_c(25073:25140)))/sqrt(length(Mu_c(25073:25140)));
sem5 = std((Muc_segment3(401:771)))/sqrt(length(Muc_segment3(401:771)));
sem6 = std((Muc_segment4(6072:9470)))/sqrt(length(Muc_segment4(6072:9470)));
sem7 =
std((Muc_segment5(9871:10510)))/sqrt(length(Muc_segment5(9871:10510)));

% error propagation of dmu calculation: take square root of sum of squares
% of sem...then divide by exact value log(V2/V1)

error2=(sqrt(sem3^2+sem2^2))/(log(V3/V2));
error3=(sqrt(sem4^2+sem3^2))/(log(V4/V3));
error4=(sqrt(sem5^2+sem4^2))/(log(V5/V4));
error5=(sqrt(sem6^2+sem5^2))/(log(V6/V5));
error6=(sqrt(sem7^2+sem6^2))/(log(V7/V6));

% a-b = duss/dln(V)
%ab1 = dmu1/(log(V2/V1));
ab2 = dmu2/(log(V3/V2));
ab3 = dmu3/(log(V4/V3));
ab4 = dmu4/(log(V5/V4));
ab5 = dmu5/(log(V6/V5));
ab6 = dmu6/(log(V7/V6));

a_b = [NaN ab2 ab3 ab4 ab5 ab6];
SV = [V2 V3 V4 V5 V6 V7];

a_b_up = [ab2 ab3 ab6];
SV_up = [V3 V4 V7];
a_b_down = [NaN ab4 ab5];
SV_down = [V2 V5 V6];
```

```
figure(4);
p1 = scatter(SV_up,a_b_up,'r','filled');
p1Children = get(p1, 'Children');
set(p1Children, 'Markersize', 20);
hold on;
p2 = scatter(SV_down,a_b_down,'r');
p2Children = get(p2, 'Children');
set(p2Children, 'Markersize', 20);
plot([-1 6],[0 0],'r');
ylim([-.025 .025]);
% xlim([0 1.68]);
xlim([-1 6]);
set(gca,'fontsize',22);
%ylabel('a-b'); xlabel('velocity (microns/second)');
%title('70 MPa effective pressure, 65 MPa pore pressure');
n=get(gca,'ytick');
set(gca,'yticklabel',sprintf('%.2f |',n'),'YMinorTick','on');
box on;


%error bars

errorbar(V3,ab2,error2),'.k';
errorbar(V4,ab3,error3,'.k');
errorbar(V5,ab4,error4,'.k');
errorbar(V6,ab5,error5,'.k');
errorbar(V7,ab6,error6,'.k');

%tex1 = text(V2,ab1,'  1');
tex2 = text(V3,ab2,'  2'); set(tex2,'Fontsize',16);
tex3 = text(V4,ab3,'  3'); set(tex3,'Fontsize',16);
tex4 = text(V5,ab4,'  4'); set(tex4,'Fontsize',16);
tex5 = text(V6,ab5,'  5'); set(tex5,'Fontsize',16);
tex6 = text(V7,ab6,'  6'); set(tex6,'Fontsize',16);
```

VTG 10

```
% moving average to smooth friction coefficient (n = 75)

for i = 1:75
    mus(i) = (mu(i));% mus = smoothed mu
end
for i = 76:n-75
    mus(i) = sum(mu(i-75:i+75))/151;
end
for i = n-74:n
    mus(i) = mu(i);
end

% moving average to smooth pore volume (n = 50)
```

```
for i = 1:50
    Pvols(i) = (Pvol(i));% mus = smoothed mu
end
for i = 51:n-50
    Pvols(i) = sum(Pvol(i-50:i+50))/101;
end
for i = n-49:n
    Pvols(i) = Pvol(i);
end


T_interest = t(13518:42360,1);
Sd_t = sd(13518:42360,1); % time appropriate shear displacement
Ad_t = ad(13518:42360,1); % axial displacement during steps
Mu_t = mu(13518:42360,1); % frictional strength during steps
Pf_t = Pf(13518:42360,1);
Pvols_i = Pvols'; % inverse of smoothed P volume
Pvols_t = Pvols_i(13518:42360,1); % smoothed P volume over velocity steps
mus_i = mus';
Mus_t = mus_i(13518:42360,1); % smoothed friction by moving average
rate = Sd_t./T_interest;
%Muc = mu -kSd_t
%y=medfilt1(Mu_t,10); % smoothed friction by median filter
% Correct slope

Mu_c = Mus_t-(((0.2643-0.2618)/(3.7-3.450)).*Sd_t)+(0.2495-0.241-.05);
Mu_c2 = Mus_t-(((0.2461-0.238)/(2.189-1.756)).*Sd_t)+(0.2424-0.2297-.1);
Mu_c3 = Mu_c-(0.026.*Sd_t)-.1+(0.8108-0.5313);
Mu_c4 = Mu_c2-.1+(0.8137-0.5631);

%%%%%%%%%%%%%%%%%%%%%%%%%%%%%%%%%%%%%%%55


figure(1);
 % Plot friction

%plot(Sd_t(1:28750),Mu_t(1:28750),'r','Color',[.57,.64,0.69]);
%hold on;
%ylabel('Friction coefficient'); xlabel('Shear displacement (mm)');
%title('10 MPa effective pressure, 125 MPa pore pressure');
xlim([0.2 6.5]);
ylim([0.4 .952]);
set(gca,'fontsize',20);
plot(Sd_t(1:28750),Mus_t(1:28750),'k');
hold on;
plot(Sd_t,Mu_c,'b');                % Plot friction w/new slope
hold on;
plot(Sd_t,Mu_c2,'g');
hold on;

plot(Sd_t(18646:28750),Mu_c3(18646:28750),'k');
hold on;
```

```
plot(Sd_t(18948:26639),Mu_c3(18948:26639),'c');
plot(Sd_t(26758:28750),Mu_c4(26758:28750),'g');

hold on;
plot(Sd_t(26958:27693),Mu_c3(26958:27693),'c');
%friction coefficient values: 0.858-0.935

% SHOW AVERAGES

% Original friction
%plot(Sd_t(8238:11159),Mus_t(8238:11159),'r');
%hold on;
%plot(Sd_t(11159:15408),Mus_t(11159:15408),'c');
%hold on;
%plot(Sd_t(16374:17086),Mus_t(16374:17086),'r');
%hold on;
%plot(Sd_t(17184:17262),Mus_t(17184:17262),'r');
hold on;
plot(Sd_t(17443:18059),Mus_t(17443:18059),'r');
% hold on;
% plot(Sd_t(18948:26639),Mus_t(18948:26639),'c');
%hold on;
%plot(Sd_t(26958:27693),Mus_t(26958:27693),'r');
%hold on;
%plot(Sd_t(27782:27869),Mus_t(27782:27869),'r');
%hold on;

% Corrected friction to slope 1
%plot(Sd_t(8238:15408),Mu_c(8238:15408),'c');
% hold on;
% plot(Sd_t(16374:17086),Mu_c(16374:17086),'r');
% hold on;
% plot(Sd_t(17184:17262),Mu_c(17184:17262),'r');
% hold on;
% plot(Sd_t(17443:18059),Mu_c(17443:18059),'r');
% hold on;
% plot(Sd_t(18948:26639),Mu_c(18948:26639),'r');
hold on;
plot(Sd_t(26958:27693),Mu_c(26958:27693),'m');
hold on;
plot(Sd_t(27782:27869),Mu_c(27782:27869),'m');

% Corrected friction to slope 2
% plot(Sd_t(4461:6992),Mu_c2(4461:6992),'c');
% hold on;
% plot(Sd_t(7400:10900),Mu_c2(7400:10900),'r');
% hold on;
% plot(Sd_t(11159:15408),Mu_c2(11159:15408),'c');
% hold on;
% plot(Sd_t(16374:17086),Mu_c2(16374:17086),'r');
% hold on;
%plot(Sd_t(17184:17262),Mu_c2(17184:17262),'r');
%hold on;
```

```
%plot(Sd_t(17443:18059),Mu_c2(17443:18059),'r');
%hold on;
%plot(Sd_t(18948:26639),Mu_c2(18948:26639),'r');
%hold on;
%plot(Sd_t(26958:27693),Mu_c2(26958:27693),'r');
%hold on;
%plot(Sd_t(27782:27869),Mu_c2(27782:27869),'r');

figure(31);
plot(Sd_t,Pvols_t);
ylabel('Pore volume (mL)'); xlabel('Shear displacement (mm)');
hold on;

% reference lines for V-steps

plot([1.679 1.679],[34.67 34.74],'r');
plot([2.269 2.269],[34.67 34.74],'r');
plot([2.741 2.741],[34.67 34.74],'g');
plot([3.319 3.319],[34.67 34.74],'g');
plot([3.852 3.852],[34.67 34.74],'r');
plot([4.399 4.399],[34.67 34.74],'r');
plot([4.925 4.925],[34.67 34.74],'g');
plot([5.464 5.464],[34.67 34.74],'g');
hold off;



%% Plot a-b

% Change in sliding velocity
% V1=0.4;
% V2=0.08;
% V3=0.8;
% V4=1.6;
% V5=0.8;
% V6=0.08;
% V7=0.8;
% V8=1.6;
% V9=0.8;

V1=0.5299294;
V2=0.1211172;
V3=1.2499073;
V4=4.9425499;
V5=1.2499073;
V6=0.1211172;
V7=1.2499073;
V8=4.9425499;
V9=1.2499073;

% VTG10
```

```
% Averages of steady state friction

mu1 = mean(Mu_c2(4461:6992));
mu2a = mean(Mu_c2(7400:10900));
mu2b = mean(Mu_c2(11159:15408));
mu3a = mean(Mu_c2(16374:17086));
mu3b = mean(Mu_c(16374:17086));
mu4 = mean(Mu_c(17184:17262));
mu5a = mean(Mu_c(17443:18059));
mu5b = mean(Mus_t(17443:18059));
mu6 = mean(Mu_c3(18948:26639));
mu7a = mean(Mu_c3(26958:27693));
mu7b = mean(Mu_c(26958:27693));
mu8 = mean(Mu_c(27782:27869));

% Diff in average coefficient of friction spanning before/after v-step
dmu1 = mean(Mu_c2(7400:10900))-mean(Mu_c2(4461:6992)); % before and after
first step
dmu2 = mean(Mu_c2(16374:17086))-mean(Mu_c2(11159:15408));
dmu3 = mean(Mu_c(17184:17262))-mean(Mu_c(16374:17086));
dmu4 = mean(Mu_c(17443:18059))-mean(Mu_c(17184:17262));
dmu5 = mean(Mu_c3(18948:26639))-mean(Mus_t(17443:18059)); % both are
incorrect
dmu6 = mean(Mu_c3(26958:27693))-mean(Mu_c3(18948:26639));
dmu7 = mean(Mu_c(27782:27869))-mean(Mu_c(26958:27693));


% STDEV of steady state friction

std1 = std(Mu_c2(4461:6992));
std2a = std(Mu_c2(7400:10900));
std2b = std(Mu_c2(11159:15408));
std3a = std(Mu_c2(16374:17086));
std3b = std(Mu_c(16374:17086));
std4 = std(Mu_c(17184:17262));
std5a = std(Mu_c(17443:18059));
std5b = std(Mus_t(17443:18059));
std6 = std(Mu_c3(18948:26639));
std7a = std(Mu_c3(26958:27693));
std7b = std(Mu_c(26958:27693));
std8 = std(Mu_c(27782:27869));

% Length of steady state friction

lengthMu1 = length(Mu_c2(4461:6992));
lengthMu2a = length(Mu_c2(7400:10900));
lengthMu2b = length(Mu_c2(11159:15408));
lengthMu3a = length(Mu_c2(16374:17086));
lengthMu3b = length(Mu_c(16374:17086));
lengthMu4 = length(Mu_c(17184:17262));
lengthMu5a = length(Mu_c(17443:18059));
lengthMu5b = length(Mus_t(17443:18059));
lengthMu6 = length(Mu_c3(18948:26639));
```

```
lengthMu7a = length(Mu_c3(26958:27693));
lengthMu7b = length(Mu_c(26958:27693));
lengthMu8 = length(Mu_c(27782:27869));

% standard error of mean at each steady state
sem1 = std1/sqrt(lengthMu1);
sem2a = std2a/sqrt(lengthMu2a);
sem2b = std2b/sqrt(lengthMu2b);
sem3a = std3a/sqrt(lengthMu3a);
sem3b = std3b/sqrt(lengthMu3b);
sem4 = std4/sqrt(lengthMu4);
sem5a = std5a/sqrt(lengthMu5a);
sem5b = std5b/sqrt(lengthMu5b);
sem6 = std6/sqrt(lengthMu6);
sem7a = std7a/sqrt(lengthMu7a);
sem7b = std7b/sqrt(lengthMu7b);
sem8 = std8/sqrt(lengthMu7b);

% error propagation of dmu calculation: take square root of sum of squares
% of sem...then divide by exact value log(V2/V1)

error1=(sqrt(sem2a^2+sem1^2))/(log(V2/V1));
error2=(sqrt(sem3a^2+sem2b^2))/(log(V3/V2));
error3=(sqrt(sem4^2+sem3b^2))/(log(V4/V3));
error4=(sqrt(sem5a^2+sem4^2))/(log(V5/V4));
error5=(sqrt(sem6^2+sem5b^2))/(log(V6/V5));
error6=(sqrt(sem7a^2+sem6^2))/(log(V7/V6));
error7=(sqrt(sem8^2+sem7b^2))/(log(V8/V7));

% a-b = duss/dln(V)
ab1 = dmu1/(log(V2/V1));
ab2 = dmu2/(log(V3/V2));
ab3 = dmu3/(log(V4/V3));
ab4 = dmu4/(log(V5/V4));
ab5 = dmu5/(log(V6/V5));
ab6 = dmu6/(log(V7/V6));
ab7 = dmu7/(log(V8/V7));

a_b = [NaN ab1 ab2 ab3 ab4 ab5 ab6 ab7];
SV = [V1 V2 V3 V4 V5 V6 V7 V8];

a_b_up = [ab2 ab3 ab6 ab7];
SV_up = [V3 V4 V7 V8];
a_b_down = [NaN ab1 ab4 ab5];          %ab4 shows the outlier...stepping down
from 1.6 to 0.8 um/s
SV_down = [V1 V2 V5 V6];
%a_b_down = [NaN ab1 ab4 ab5];
%SV_down = [V1 V2 V5 V6];

figure(2);
p1 = scatter(SV_up,a_b_up,'g','filled');
p1Children = get(p1, 'Children');
set(p1Children, 'Markersize', 20);
```

```
hold on;
p2 = scatter(SV_down,a_b_down,'g');
p2Children = get(p2, 'Children');
set(p2Children, 'Markersize', 20);
plot([-1 6],[0 0],'r')
% xlim([0 1.68]);
xlim([-1 6]);
ylim([-.025 .025]);
set(gca,'fontsize',22);
%ylabel('a-b'); xlabel('velocity (microns/second)');
%title('10 MPa effective pressure, 125 MPa pore pressure');
%title('Velocity dependence of friction at 135:125 MPa (Pc:Pf)');
n=get(gca,'ytick');
set(gca,'yticklabel',sprintf('%.2f |',n'),'YMinorTick','on');
box on;

%error bars
errorbar(V2,ab1,error1,'.k');
errorbar(V3,ab2,error2),'.k';
errorbar(V4,ab3,error3,'.k');
errorbar(V5,ab4,error4,'.k');
errorbar(V6,ab5,error5,'.k');
errorbar(V7,ab6,error6,'.k');
errorbar(V8,ab7,error7,'.k');

tex1 = text(V2,ab1,'   1'); set(tex1,'Fontsize',16);
tex2 = text(V3,ab2,'   2'); set(tex2,'Fontsize',16);
tex3 = text(V4,ab3,'   3'); set(tex3,'Fontsize',16);
tex4 = text(V5,ab4,'   4'); set(tex4,'Fontsize',16);
tex5 = text(V6,ab5,'   5'); set(tex5,'Fontsize',16);
tex6 = text(V7,ab6,'   6'); set(tex6,'Fontsize',16);
tex7 = text(V8,ab7,'   7'); set(tex7,'Fontsize',16);
```